



HAL
open science

Extended aerosol and surface characterization from S5P/TROPOMI with GRASP algorithm. Part II: Global validation and Intercomparison

Cheng Chen, Pavel Litvinov, Oleg Dubovik, Lukas Bindreiter, Christian Matar, David Fuertes, Anton Lopatin, Tatyana Lapyonok, Verena Lanzinger, Andreas Hangler, et al.

► To cite this version:

Cheng Chen, Pavel Litvinov, Oleg Dubovik, Lukas Bindreiter, Christian Matar, et al.. Extended aerosol and surface characterization from S5P/TROPOMI with GRASP algorithm. Part II: Global validation and Intercomparison. Remote Sensing of Environment, 2024, 313, pp.114374. 10.1016/j.rse.2024.114374 . hal-04763296

HAL Id: hal-04763296

<https://hal.science/hal-04763296v1>

Submitted on 2 Nov 2024

HAL is a multi-disciplinary open access archive for the deposit and dissemination of scientific research documents, whether they are published or not. The documents may come from teaching and research institutions in France or abroad, or from public or private research centers.

L'archive ouverte pluridisciplinaire **HAL**, est destinée au dépôt et à la diffusion de documents scientifiques de niveau recherche, publiés ou non, émanant des établissements d'enseignement et de recherche français ou étrangers, des laboratoires publics ou privés.



Distributed under a Creative Commons Attribution 4.0 International License



Extended aerosol and surface characterization from S5P/TROPOMI with GRASP algorithm. Part II: Global validation and Intercomparison

Cheng Chen^{a,g,*}, Pavel Litvinov^{a,*}, Oleg Dubovik^b, Lukas Bindreiter^c, Christian Matar^a, David Fuertes^a, Anton Lopatin^a, Tatyana Lapyonok^b, Verena Lanzinger^c, Andreas Hangler^c, Michael Aspetsberger^c, Martin de Graaf^d, Lieuwe Gijsbert Tilstra^d, Piet Stammes^d, Alexandru Dandocsi^e, Daniele Gasbarra^f, Elody Fluck^e, Claus Zehner^e, Christian Retscher^e

^a GRASP SAS, Remote Sensing Developments, 3 rue Louis Néel, 59260 Lezennes, France

^b Univ. Lille, CNRS, UMR 8518 - LOA - Laboratoire d'Optique Atmosphérique, F-59000 Lille, France

^c Cloudflight, 23 Huemerstrasse, Linz, Austria

^d KNMI, Utrechtseweg 297, De Bilt, the Netherlands

^e ESA-ESRIN, 1 Via Galilei, Frascati 00044, Italy

^f Shamrock Space Services, c/o ESA-ESRIN, 1 Via Galilei, Frascati 00044, Italy

^g Anhui Institute of Optics and Fine Mechanics, Hefei Institutes of Physical Science, Chinese Academy of Sciences, Hefei 230031, China

ARTICLE INFO

Editor: Menghua Wang

Keywords:

Sentinel-5P/TROPOMI
Satellite remote sensing
Aerosol and surface characterization
Validation and inter-comparison

ABSTRACT

This paper is the second part of companion papers describing the development of GRASP approach for aerosol and surface retrieval from Sentinel-5P/TROPOMI. Here we focus on the S5P/TROPOMI GRASP aerosol and surface products global validation and systematic intercomparison with other products from independent instruments and algorithms. Specifically, we have validated the S5P/TROPOMI GRASP, Suomi-NPP/VIIRS DB and MODIS/TERRA DT + DB aerosol products with the ground-based AERONET referenced measurements using the same methodology and intercompare the validation results. In addition, the global pixel-to-pixel inter-comparisons of the aerosol products (AOD, fine/coarse mode AOD and SSA) are performed over different surfaces, i.e., ocean and land surface with different NDVIs. Besides, we compared the S5P/TROPOMI GRASP, MODIS MCD43 surface BRDF/albedo as well as OMI, GOME-2 and SCIAMACHY Lambertian-Equivalent Reflectivity (LER) albedo climatology developed by Royal Netherlands Meteorological Institute (KNMI) with the surface reference dataset generated based on the synergetic retrieval of AERONET and S5P/TROPOMI measurements. Finally, the inter-comparisons of the surface BRDF and albedo datasets were performed globally at the UV, VIS, NIR and SWIR parts of the spectrum. Overall, generally good agreement was observed between independent aerosol and surface datasets with a high percentage of pixels satisfying the Optimal and Target requirements. We would emphasize two advantages for TROPOMI/GRASP aerosol and surface products: (i) it provides spectral AOD together with detailed aerosol properties, such as fine/coarse mode AOD, spectral AAOD and SSA at UV, VIS, NIR and SWIR wavelengths, which are important for constraining aerosol environmental and climate effects; (ii) the TROPOMI/GRASP aerosol and surface products are globally retrieved simultaneously in a fully consistent manner.

1. Introduction

Understanding the role of atmospheric aerosol burden as well as its spatial and temporal variability plays an important role in many research fields, such as the aerosol direct and indirect effects on the Earth-atmosphere system radiation budget, air pollution effects on

human health (Pöschl, 2005; Forster et al., 2021; Chen et al., 2022a), and aerosol effects on the ecosystems (Kulmala et al., 2004; Mahowald et al., 2017). In the last 2 decades, satellite remote sensing has been proven to be the key technology contributing to these research fields by providing continuous and large-scale coverage atmospheric aerosol observations (Dubovik et al., 2021b; Kaufman et al., 2002; King et al.,

* Corresponding authors at: GRASP SAS, Remote Sensing Developments, 3 rue Louis Néel, 59260 Lezennes, France.

E-mail addresses: cheng.chen@aiofm.ac.cn (C. Chen), pavel.litvinov@grasp-sas.com (P. Litvinov).

<https://doi.org/10.1016/j.rse.2024.114374>

Received 22 December 2023; Received in revised form 15 August 2024; Accepted 15 August 2024

Available online 20 August 2024

0034-4257/© 2024 The Authors. Published by Elsevier Inc. This is an open access article under the CC BY license (<http://creativecommons.org/licenses/by/4.0/>).

1999; Li et al., 2009). Led by NASA, ESA and other space agencies, a diversity of satellite instruments has been deployed in the orbits (i.e. sun-synchronous and geo-synchronous) to monitor atmospheric aerosol and deliver the product to the relevant users and research community. For example, as part of NASA EOS mission, MODIS, MISR and OMI instruments have continuously generated aerosol products since the end of the last century (Diner et al., 1998; King, 1999; Levelt et al., 2006; Salomonson et al., 2002; Wielicki et al., 1995). The VIIRS instrument onboard of the Suomi National Polar-orbiting Partnership (Suomi-NPP) and NOAA-20 satellites was launched in 2011 and 2017 respectively to continue EOS MODIS measurements (Cao et al., 2013, 2018). MERIS and AATSR instruments onboard of ESA's ENVISAT mission (Rast et al., 1999; Lewellyn-Jones et al., 2001) were operational from 2002 to 2012 and the mission has been replaced by the Sentinel series of satellites.

A series of retrieval algorithms have been developed to derive aerosol information from the space-borne instruments' Top-Of-Atmosphere (TOA) measurements, such as Dark Target (DT), Deep Blue (DB) and Multi-Angle Implementation of Atmospheric Correction (MAIAC) algorithms which are applied for operational processing of MODIS and VIIRS observations (Hsu et al., 2019; Hsu et al., 2013; Hsu et al., 2004; Kaufman et al., 1997; Levy et al., 2015; Levy et al., 2007; Lyapustin et al., 2018; Remer et al., 2005; Sayer et al., 2018a; Tanré et al., 1997). Under the ESA Climate Change Initiative (CCI) project, several aerosol remote sensing algorithms are developed for ESA missions (de Leeuw et al., 2015; Holzer-Popp et al., 2013; Popp et al., 2016). Many previous studies have conducted comprehensively validation and intercomparison of these conventional aerosol remote sensing datasets (Bréon et al., 2011; Chen et al., 2020; Kokhanovsky et al., 2010; Kokhanovsky et al., 2007; Li et al., 2020; Schutgens et al., 2020; Soga-cheva et al., 2020). On one hand, most studies focus on the AOD at visible channels, in particular, mid-visible 550 nm, which is due to the fact that the algorithms are largely tuned to AOD (550 nm). The knowledge of AOD consistency at wider spectrum range and for more detailed aerosol properties (i.e. size, absorption etc.) are somewhat limited (Chen et al., 2020; Schutgens et al., 2021). On the other hand, there is lack of studies on fine resolution pixel-to-pixel inter-comparison of aerosol products. Furthermore, atmosphere-surface decoupling is the main challenge of quantitatively remote sensing of the Earth-atmosphere system. However, in order to separate surface and atmosphere signals, most of the aerosol remote sensing algorithms are relying on a priori knowledge of the surface climatology (i.e. DB) (Hsu et al., 2013) or empirical assumption of surface reflectance between SWIR and VIS channels over dense vegetation area (i.e. DT) (Kaufman et al., 1997). As a consequence, the aerosol and surface products are derived using independent algorithms, which may produce certain inconsistency for the Earth-atmosphere radiation calculation from these data.

As described in Part I (Litvinov et al., 2024), with proper adaptation of forward (aerosol and surface models) and inversion approaches (single and multi-pixel constraints), GRASP algorithm (Dubovik et al., 2021a; Dubovik et al., 2014; Dubovik et al., 2011) allows simultaneous retrieval of the aerosol and surface from S5P/TROPOMI measurements. In particular, besides traditional spectral AOD, TROPOMI/GRASP provides extended aerosol and surface characterization, such as spectral fine/coarse mode AOD, AAOD, SSA as well as full Bidirectional Reflectance Distribution Function (BRDF) and surface albedos at 10 wavelengths covering UV, VIS, NIR and SWIR spectrum. The objective of this paper, as the Part I companion paper, is to comprehensive investigation of the consistency and discrepancy in aerosol and surface between TROPOMI/GRASP and the conventional products, including VIIRS/DB (Hsu et al., 2019; Sayer et al., 2018a, 2018b) and MODIS/TERRA DT + DB merged (Levy et al., 2013; Sayer et al., 2014) aerosol products and MODIS/MCD43 BRDF/albedo products (Schaaf and Wang, 2015a, 2015b) as well as OMI, GOME-2 and SCIAMACHY Lambertian-Equivalent Reflectivity (LER) albedo climatology developed by the Royal Netherlands Meteorological Institute (KNMI) (Kleipool et al., 2008; Tilstra et al., 2021; Tilstra et al., 2017). We describe the global

aerosol and surface datasets used in this study in Section 2. Section 3 describes the validation of aerosol and surface datasets with the ground-based reference datasets and the intercomparison of the validation results. Section 4 illustrates the pixel level intercomparison of the aerosol and surface products. Section 5 summarizes and discusses the lessons learned and concludes the study.

2. Global aerosol and surface datasets

2.1. Aerosol datasets

In this section, the main aerosol products used in this study are described. A brief summary of these datasets is given in Table 1.

2.1.1. S5P/TROPOMI GRASP aerosol product

The Tropospheric Monitoring Instrument (TROPOMI) aboard the Sentinel-5 Precursor (S5P) satellite was launched on 13 October 2017. The TROPOMI instrument (Veeffkind et al., 2012) is a spectrometer that measures top-of-atmosphere (TOA) high spectral resolution (0.25–1 nm) radiances at UV, VIS, NIR and SWIR with a swath of about 2600 km crossing the equator (ascending orbit) at 13:30 PM mean local time. The typical spatial resolution at nadir is $5.5 \times 3.5 \text{ km}^2$ with exception of the UV1 ($5.5 \times 28 \text{ km}^2$) and SWIR ($5.5 \times 7 \text{ km}^2$). S5P/TROPOMI measured TOA radiances at 10 selected wavelengths from UV to SWIR (340, 367, 380, 416, 440, 494, 670, 747, 772, and 2313 nm) are inverted using GRASP/Models approach (Litvinov et al., 2024 Part I), where the aerosol is represented by external mixture of several AERONET climatological models with prescribed spectral dependencies of the complex refractive index, size distribution and non-sphericity. The single scattering characteristics in GRASP/Models approach are presented with aerosol simulation as external mixture of climatological aerosol models (Chen et al., 2020; Lopatin et al., 2021; Dubovik et al., 2021a). While GRASP/Models approach is rather simple it shows to be very efficient being applied to satellite measurements, especially by instruments with limited information content (Chen et al., 2020, 2022b). Specifically, 4 aerosol models (fine absorbing (biomass burning), fine slightly absorption (urban), coarse mode maritime (oceanic) and coarse mode dust (dust)) concentrations and layer height are directly retrieved together with land/ocean surface BRDF parameters. Then the AOD, AODF, AODC, SSA and AAOD at 10 wavelengths are derived products and used in this study for intercomparison with other independent aerosol datasets. The S5P/TROPOMI GRASP aerosol product has a 0.09° ($\sim 10 \times 10 \text{ km}^2$) spatial resolution (close to the native resolution in SWIR channel) under equidistant cylindrical projection with WGS84 coordinate system.

2.1.2. MODIS/TERRA DT + DB aerosol product

NASA's Moderate Resolution Imaging Spectroradiometer (MODIS) aboard on the TERRA satellite crossing equator (descending orbit) at 10:30 AM mean local time measures TOA radiances at 36 spectral bands from 0.4 to $14.4 \mu\text{m}$ in a sun-synchronous orbit with 2330 km wide viewing swath. This information has been widely used for atmosphere, land and ocean applications since TERRA was launched in 1999 and expected to stop operating in 2025 due to the orbital drift. Numerous algorithms have been developed to extract aerosol information from MODIS data. NASA distributes three operational MODIS aerosol datasets: Dark Target (DT) by Remer et al. (2005) and Levy et al. (2013), Deep Blue (DB) by Hsu et al. (2004, 2006, 2013), and Multi-Angle Implementation of Atmospheric Correction (MAIAC) by Lyapustin et al. (2018). However, the DT algorithm cannot be used over bright surfaces (e.g. desert, arid and semi-arid surfaces), where the DB algorithm was originally developed to fill in, although the enhanced DB algorithm has been extended to all land surfaces (Hsu et al., 2013). Therefore, the DT and DB AOD (550 nm) is combined into a novel dataset to provide better coverage over land and ocean (Levy et al., 2013; Sayer et al., 2014). In this study, MODIS/TERRA Level 2 aerosol dataset is adopted for the intercomparison purpose. Specifically, the

Table 1
Global aerosol products used in this study.

Sensor	Algorithm (Version)	Resolution	Variables
S5p/TROPOMI	GRASP (v1.1.0)	10 km	AOD, AODF, AODC, AAOD, SSA at 10 wavelengths (340, 367, 380, 416, 440, 494, 670, 747, 772, and 2313 nm)
MODIS/TERRA	DT + DB Merged (C6.1)	nadir 10 km	AOD (550 nm)
Suomi-NPP/ VIIRS	DB (v1.1)	6 km	AOD (412 nm) – Land only AOD at 490, 550 and 670 nm AODF, AODC (550 nm) – Ocean only SSA at 412, 490 and 670 nm – Land only
Sun-photometer/ AERONET	Version 3 (Level 2.0)	Ground-based point measurement	Direct-Sun AOD at 440, 675, 870 and 1020 nm SDA AODF/AODC at 500 nm Inversion SSA at 440, 675, 870 and 1020 nm

MOD04 Collection 6.1 DT + DB combined AOD (550 nm) products is used. The spatial resolution of this product is 10 km at nadir and ~50 km near the edges of the swath.

2.1.3. Suomi-NPP/VIIRS DB aerosol product

Visible Infrared Imaging Radiometer Suite (VIIRS) aboard on the Suomi National Polar-orbiting Partnership (Suomi-NPP) satellite (Cao et al., 2013) launched in 2011 and NOAA-20 satellite launched in 2017 (Cao et al., 2018) is dedicated to continue the Earth Observing System (EOS) MODIS aerosol products to the Joint Polar Satellite System (JPSS) VIIRS and extend the long-term aerosol dataset. VIIRS measures TOA radiances at 22 spectral bands from 0.41 to 12.5 μm in a sun-synchronous orbit crossing the equator (ascending orbit) at 1:30 PM mean local time with a 3060 km wide viewing swath. Since S5P flies within ~3–5 minutes of Suomi-NPP, the synergy between VIIRS and TROPOMI allows to support the TROPOMI cloud identification using the high spatial resolution measurements of VIIRS (375 to 750 m) (Veefkind et al., 2012). The recent application of DB algorithm for VIIRS aerosol retrieval (Hsu et al., 2019) shows good performance, and the Satellite Ocean Aerosol Retrieval (SOAR) algorithm is integrated into the DB algorithm to extend VIIRS DB aerosol dataset over ocean (Sayer et al., 2018a, 2018b). In this study, the Suomi-NPP VIIRS DB 6 km Level 2 aerosol product (AERDB_L2_VIIRS_SNPP) is used to intercompare with the TROPOMI/GRASP and MODIS/TERRA DT + DB aerosol products. The AERDB_L2_VIIRS_SNPP aerosol dataset includes spectral AOD at 412, 490, 550 and 670 nm over land and AOD at 490, 550 and 670 nm over ocean. The fine mode fraction at 550 nm is also provided over ocean that can be used to derive AODF and AODC at 550 nm. Over land, the diagnosed spectral SSA at 412, 490 and 670 nm are also included in the intercomparison.

2.1.4. AERONET ground-based aerosol reference dataset

The Aerosol Robotic Network (AERONET) is a global distributed ground-based aerosol measurement network. This infrastructure has maintained uninterrupted operational functionality for >28 years using well-calibrated sun-sky photometers (Holben et al., 1998). The AERONET direct-Sun spectral AOD is with reliable accuracy (0.01–0.02) (Eck et al., 1999), which are widely used as “ground truth” to validate remote sensing aerosol products and aerosol model simulations. In addition, the sun-sky photometers measure sky diffuse radiation that is used to invert detailed aerosol properties, such as size distribution, complex refractive index, single scattering albedo, and non-sphericity etc., which provide insights of aerosol microphysics (Dubovik and King, 2000; Dubovik et al., 2006). The accuracy of AERONET inversion products has been analyzed by Dubovik et al. (2000) and Sinyuk et al. (2020). Both AERONET direct-Sun and inversion products are considered as the ground-based reference dataset and support the climate model evaluation and form the aerosol model climatology used in the satellite retrieval algorithm (Dubovik et al., 2002). In this study, the up-to-date AERONET Version 3 Level 2.0 (Smirnov et al., 2000; Giles et al., 2019) direct-Sun AOD, the spectral deconvolution algorithm (SDA) fine/coarse mode

AOD (O’Neill et al., 2003), and inverted SSA products (last access: 2021-06-25) are used. We make use of all AERONET sites with available data during the study period.

2.2. Surface datasets

In this section, the surface datasets used for validation and inter-comparison are described. Table 2 shows a brief description of the surface products used in this study.

2.2.1. S5P/TROPOMI GRASP surface product

As described in Part I (Litvinov et al., 2024), the GRASP algorithm retrieves aerosol and full surface BRDF simultaneously. With the full BRDF parameters, the surface characteristics can be derived such as vegetation indexes, white sky albedo (BHR_ISO) and black sky albedo (DHR) covering TROPOMI UV, VIS, NIR to SWIR bands. Specifically, the S5P-TROPOMI/GRASP retrieval is based on Ross-Li land BRDF model (Ross, 1981; Li and Strahler, 1992) with modifications by Litvinov et al. (2011a, 2011b) to treat only spectral dependent isotropic term while the volumetric and geometric terms are considered spectrally independent. The Cox-Munk model (Cox and Munk, 1954) consideration of spectral dependence of foam/whitecaps albedo (Frouin et al., 1996; Frouin and Pelletier, 2015) is used for the ocean surface BRDF calculation. Meanwhile, the angular ocean surface BRDF is constrained using the wind speed near the surface based on empirical relationships (Cox and Munk, 1954; Monahan and O’Muircheartaigh, 1980; Koepke, 1984; Frouin and Pelletier, 2015).

2.2.2. MODIS surface product

The MODIS Collection 6 Bidirectional Reflectance Distribution Function and Albedo Model Parameters produced in a 0.05° climate model grid datasets (MCD43C) are used in the intercomparison. Specifically, MCD43C1 provides three BRDF model weighting parameters (isotropic, volumetric and geometric terms) (Schaaf and Wang, 2015a) and MCD43C3 contains the surface albedos (white sky albedo and black sky albedo) (Schaaf and Wang, 2015b). MODIS and TROPOMI/GRASP are based on the same Ross-Li BRDF model with some differences described in the Part I of papers (Litvinov et al., 2024). Such products of BRDF as isotropic, volumetric and geometric terms as well as surface albedos will be directly intercompared in this paper.

MCD43C product is provided at spectral bands 1–7 covering VIS to SWIR, however there are only 2 bands (blue and red) overlapped (center wavelength within 20 nm) with TROPOMI/GRASP surface product, and the intercomparison will be performed at these 2 bands. By considering that (i) MCD43C products is produced on the basis of 16 days accumulation of TERRA and AQUA MODIS data and temporally weighted to the day of interest, and (ii) surface generally varies slowly in time, the MODIS and TROPOMI surface intercomparison will be done on the monthly mean characteristics.

Table 2
Global surface products used in this study.

Sensor	Product or Algorithm (Version)	Resolution	Variables
S5p/TROPOMI	GRASP (v1.1.0)	10 km	Full BRDF, DHR and BHR_ISO at 10 wavelengths (340, 367, 380, 416, 440, 494, 670, 747, 772, and 2313 nm)
MODIS TERRA+AQUA	MCD43C1 and MCD43C3	0.05 degree	Full BRDF, black/white sky albedo at 7 wavelengths from blue to SWIR
OMI	KNMI LER Climatology ¹	0.5 degree	Lambertian-Equivalent Reflectivity (LER) at 23 wavelengths from UV to green, 6 of them are selected (342, 367, 380, 416, 440 and 494 nm) for intercomparison
GOME-2	KNMI LER v3.1 Climatology ²	0.25 degree	LER at 26 wavelengths from UV to NIR, 9 of them are selected (340, 367, 380, 416, 440, 494, 670, 758, 772 nm)
SCIAMACHY	KNMI LER v2.6 Climatology ³	0.5 degree	LER at 34 wavelengths from UV to SWIR, 10 of them are selected (340, 367, 380, 416, 440, 494, 670, 758, 772, 2314 nm)
Surface reference (S5p/TROPOMI)	TROPOMI + AERONET combined retrieval GRASP (v1.1.0) ⁴	30 km (3 × 3 10 km pixels) region over 30 AERONET sites	Full BRDF, DHR (black sky albedo) and BHR_ISO (white sky albedo) at 10 wavelengths (340, 367, 380, 416, 440, 494, 670, 747, 772, and 2313 nm)

¹ https://www.temis.nl/surface/albedo/omi_ler.php (Kleipool et al., 2008; Tilstra et al., 2017).

² https://www.temis.nl/surface/albedo/gome2_ler.php (Tilstra et al., 2017, 2021).

³ https://www.temis.nl/surface/albedo/scia_ler.php (Tilstra et al., 2017).

⁴ <https://www.grasp-open.com/products/grosat-data-release/> (Litvinov et al., 2022).

2.2.3. SCIAMACHY, OMI and GOME-2 surface LER climatology

The SCIAMACHY, OMI and GOME-2 surface Lambertian-Equivalent Reflectivity (LER) albedo climatology datasets generated by KNMI (Royal Netherlands Meteorological Institute) (Kleipool et al., 2008; Tilstra et al., 2017, 2021) covering from UV to SWIR are also included in the intercomparison. The KNMI SCIAMACHY, OMI and GOME-2 LER climatology are provided for each month of the year by accumulating several years of observations (for example, OMI LER is based on data obtained from 2004 to 2007, and 2008–2018 for GOME-2 LER and 2002–2012 for SCIAMACHY LER). The LER albedos are all provided at 1 nm wavelength bins with spatial resolutions of 0.25 to 0.5°, respectively. OMI covers from UV to VIS spectrum, and GOME-2 covers from UV, VIS to NIR, and SCIAMACHY further extends to SWIR channels. In this study, we consider the center wavelength within 20 nm to be overlapped, therefore several common wavelengths (Table 2) are selected in order to intercompare with TROPOMI.

2.2.4. S5P/TROPOMI surface reference dataset

The S5P/TROPOMI reference surface dataset is generated by employing the concept of the synergy retrieval of the combination of AERONET and S5P/TROPOMI measurements within the framework of ESA GROSAT project (<https://www.grasp-sas.com/projects/grosat/>). The AERONET almucantar radiance within 6 h of S5P overpass and direct sun AOD measurements within 60 mins of S5P overpass are combined with S5P/TROPOMI measured radiances collocated with 30 km region of AERONET stations. The GRASP algorithm retrieves aerosol and surface parameters by fitting the combined measurements. The GRASP multi-pixel concept allows for deriving the extended aerosol microphysical and optical properties mainly from AERONET almucantar and direct sun measurements which are of rich information content due to multi-angular and multi-spectral measurements in forward scattering. Meanwhile, the surface properties are retrieved largely relying on satellite measurements. Once the inversion is converged with small fitting residual of S5P/TROPOMI measurements and the derived aerosol properties are with good agreement with AERONET, the surface product can be considered as the reference dataset (Litvinov et al., 2020; Litvinov et al., 2022). We generated one-year S5P/TROPOMI reference surface dataset (<https://www.grasp-open.com/products/grosat-data-release/>) of 3 × 3 pixels (~30 km region) over selected 30 AERONET sites covering different aerosol and surface types that are used in this study.

3. Intercomparison of validation with aerosol and surface reference datasets

The S5P/TROPOMI GRASP aerosol and surface products validation has been performed in Part I (Litvinov et al., 2024). In this section, to demonstrate the place of TROPOMI/GRASP aerosol and surface products among other widely used ones, we intercompare the satellite

remote sensing aerosol and surface products validation metrics with the reference datasets. Specifically, we evaluate the S5P/TROPOMI GRASP, Suomi-NPP/VIIRS DB and MODIS/TERRA DT + DB combined aerosol products with AERONET over the same time period using the same matchup methodology and compare the validation metrics. As for the surface, the S5P/TROPOMI GRASP and MODIS (TERRA+AQUA) monthly surface products as well as OMI, GOME-2 and SCIAMACHY surface LER climatology are evaluated with S5P/TROPOMI surface reference dataset and the validation metrics are then intercompared.

3.1. Intercomparison of validation of aerosol products with AERONET

3.1.1. Intercomparison of AOD products validation with AERONET

In order to validate AOD products with AERONET, we follow the same matchup strategy as in Chen et al. (2020) that the gridded satellite high-quality retrievals are averaged in a 3 × 3 pixels window centered over the AERONET stations. Only pure land/ocean pixels are taken into account and the minimal 50% coverage of satellite pixels within a window is adopted as the acceptance threshold. All available AERONET Level 2 direct-sun AODs (last access: 2021-06-25) are averaged within +/- 30 mins of satellite overpass time. The quality assurance index (QA) is used to select high-quality retrieval products to perform validation. TROPOMI/GRASP QA index definition and analysis is described in the Part I of the papers (Litvinov et al., 2024). MODIS and VIIRS QA indices are described in Hubanks (2017), Sayer et al. (2018a) and Hsu et al. (2019). Specifically, to select the best quality pixels and have comparable number of matching-up points with AERONET, over land the QA = 3 is taken for TROPOMI/GRASP and MODIS/TERRA DT + DB, and QA ≥ 2 for VIIRS/DB. Over ocean QA ≥ 2 is used for all 3 products. The Ångström exponent (AE or $\alpha = \frac{\ln\tau_2 - \ln\tau_1}{\ln\lambda_1 - \ln\lambda_2}$, where λ represents wavelength and τ is AOD) is used to interpolate TROPOMI/GRASP and AERONET AOD to the 4 common wavelengths (412, 490, 550 and 670 nm) with MODIS/TERRA DT + DB and VIIRS/DB products for validation and intercomparison. For quantifying the validation results, we follow Chen et al. (2020) for the statistical parameters, such as Pearson correlation coefficient (R), root mean square error (RMSE), GCOS fraction (%), Slope, Offset of linear regression, and biases for total (BIAS), low (BIAS_{AOD<0.2}), medium (BIAS_{0.2≤AOD≤0.7}) and high (BIAS_{AOD>0.7}) AODs. In addition, we include the Target fraction (%) that describes the percentage of AOD retrievals satisfying the AOD Target requirement: max (0.05 or 20% AOD) (Litvinov et al., 2024). The Target requirement is a bit loose with respect to the GCOS requirement: max (0.05 or 20% AOD) vs. max (0.04 or 10% AOD).

Fig. 1 shows the mid-visible AOD (550 nm) validation results for TROPOMI/GRASP, VIIRS/DB and MODIS/DT + DB over land for one year period March 2019 to February 2020. The total matchup points are comparable for 3 products: TROPOMI/GRASP (7732), VIIRS/DB (7940)

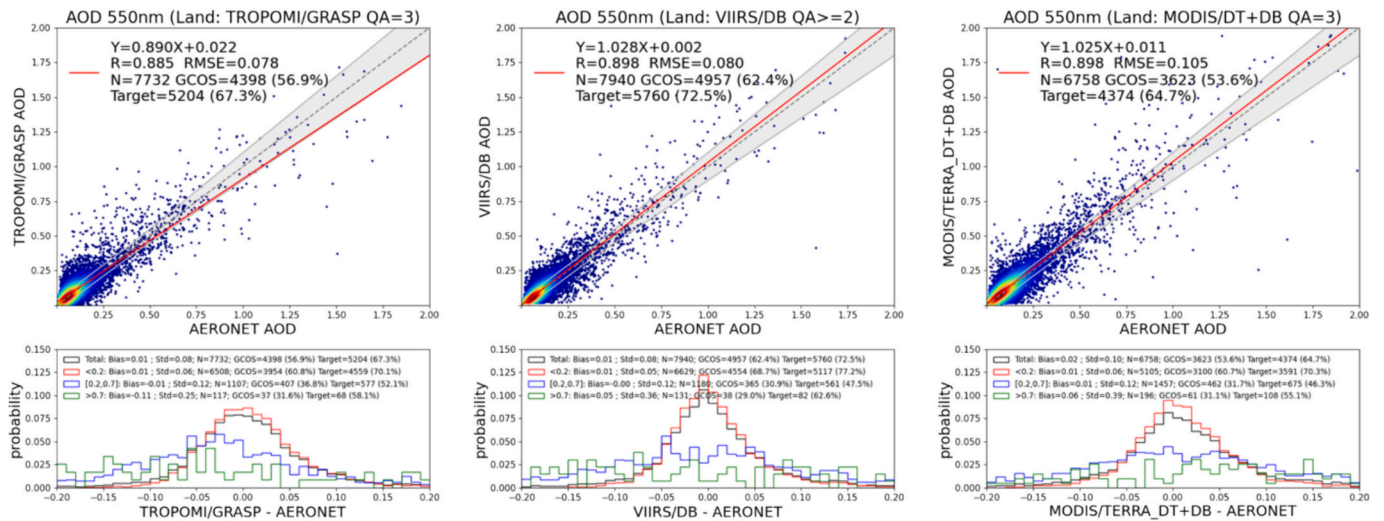


Fig. 1. Validation of TROPOMI/GRASP, VIIRS/DB and MODIS/TERRA DT + DB AOD 550 nm over land with AERONET for an entire year (March 2019 to February 2020). The gray dashed line and the red solid line are the 1:1 reference line and the linear regression line. The gray envelope indicates GCOS requirement max (0.04 or 10% AOD). The probability density function of differences between satellite and AERONET AOD and the Bias under different AOD conditions (any AOD, AOD < 0.2, 0.2 ≤ AOD ≤ 0.7 and AOD > 0.7) are present in the lower panels. (For interpretation of the references to colour in this figure legend, the reader is referred to the web version of this article.)

and MODIS/DT + DB (6758). The 3 AOD (550 nm) products show good agreement with AERONET with correlation coefficient (R) around 0.88–0.90. TROPOMI/GRASP (0.078) and VIIRS/DB (0.080) shows slightly better RMSE than MODIS/DT + DB (0.105). VIIRS/DB is of a little bit better GCOS (62.4%) and Target (72.5%) fractions than TROPOMI/GRASP (GCOS: 56.9%; Target: 67.3%) and MODIS/DT + DB (GCOS: 53.6%; Target: 64.7%). In terms of biases, 3 products show similar bias (+0.01) for low AOD ($BIAS_{AOD<0.2}$), and for total BIAS MODIS/DT + DB (+0.02) is slightly larger than TROPOMI/GRASP (+0.01) and VIIRS/DB (+0.01). While the biases for high AOD ($BIAS_{AOD>0.7}$) are of large difference that VIIRS/DB and MODIS/DT + DB show overestimation around 0.05–0.06, in contrast TROPOMI/GRASP tends to underestimate around 0.11.

Table 3 summarizes TROPOMI/GRASP, VIIRS/DB and MODIS/TERRA DT + DB spectral AOD (412, 490, 550 and 670 nm) validation metrics with AERONET over land. In this study, we use MODIS/TERRA DT + DB combined AOD product, which is of better coverage than individual DT or DB products while DT + DB combined AOD is only available at mid-visible (550 nm). For VIIRS/DB, 4 bands AOD (412, 490, 550 and 670 nm) is provided over land. TROPOMI/GRASP and VIIRS/DB show similar performance from 412 to 670 nm. Generally, VIIRS/DB shows slightly higher GCOS and Target fractions and a bit larger dispersion (RMSE) than TROPOMI/GRASP. The BIAS and $BIAS_{AOD<0.2}$ do not exceed 0.02 for both of them from deep blue (412 nm) to red (670 nm) channels. However, the spectral tendency is opposite, that TROPOMI/GRASP BIAS decreases from +0.02 at 412 nm to 0.00 at 670 nm, while VIIRS/DB BIAS slightly increases from 0.00 at

412 nm to +0.01 at 670 nm.

Table 4 shows the TROPOMI/GRASP, VIIRS/DB and MODIS/TERRA DT + DB AOD 550 nm validation metrics with AERONET over four classes of land surface ($0 < NDVI \leq 0.2$, $0.2 < NDVI \leq 0.4$, $0.4 < NDVI \leq 0.6$, and $0.6 < NDVI \leq 1$). Previous studies have indicated the satellite AOD products show different performance over different land surfaces (Sayer et al., 2013; Sayer et al., 2014; Chen et al., 2020), especially over bare soil/desert surfaces ($0 < NDVI \leq 0.2$) the discrepancy between the products is much larger than over other surface types (Chen et al., 2020). Even though, the best R is observed for TROPOMI/GRASP over bare soil/desert surfaces ($0 < NDVI \leq 0.2$), the highest BIAS and $BIAS_{AOD<0.2}$ (0.06–0.07) is also present. Moreover, TROPOMI/GRASP show the smallest BIAS and $BIAS_{AOD<0.2}$ as well as the smallest dispersion (RMSE) over 3 classes of $NDVI > 0.2$. VIIRS/DB show good GCOS and Target fractions, specifically > 50% GCOS at all surface types. The most of matchups for 3 products (TROPOMI/GRASP - 86%, VIIRS/DB - 89%, MODIS/TERRA DT + DB - 85%) are located in the middle range of NDVI ($0.2 < NDVI \leq 0.6$), where the retrieval algorithm generally performs well. In the dense vegetation area ($0.6 < NDVI \leq 1$), all 3 products show relatively low R (<0.85), which is due to the fact that there are largely low and moderate AOD conditions, therefore the dispersion (RMSE) is relatively small with respect to the other areas. The relatively low GCOS and Target fractions over bright surface ($0 < NDVI \leq 0.2$) are consistent with Chen et al. (2020) and are due to the general difficulty of aerosol and surface decoupling over bright surface where the surface contribution is dominant.

Fig. 2 shows the validation of TROPOMI/GRASP, VIIRS/DB and

Table 3

Summary of TROPOMI/GRASP, VIIRS/DB and MODIS/TERRA DT + DB spectral AOD validation metrics with AERONET reference dataset over land. The best performing metric is indicated in bold.

Land/Ocean	Bands (nm)	Products (Num. Matchups)	R	Slope	Offset	RMSE	BIAS	BIAS AOD < 0.2	GCOS (%)	Target (%)	
Land	412	TROPOMI (7732)	0.887	0.920	0.035	0.115	0.02	0.02	41.8	53.9	
		VIIRS (6528)	0.914	1.074	-0.013	0.119	0.00	0.00	50.8	61.8	
	490	TROPOMI (7732)	0.889	0.905	0.026	0.089	0.01	0.02	50.8	62.3	
		VIIRS (7940)	0.900	1.050	0.000	0.094	0.01	0.01	57.5	67.9	
	550	TROPOMI (7732)	0.885	0.890	0.022	0.078	0.01	0.01	56.9	67.3	
		VIIRS (7940)	0.898	1.028	0.002	0.080	0.01	0.01	62.4	72.5	
	670	MODIS (6758)	0.898	1.025	0.011	0.105	0.02	0.01	53.6	64.7	
		TROPOMI (7732)	0.877	0.835	0.018	0.065	0.00	0.01	66.4	76.1	
			VIIRS (7940)	0.885	0.979	0.008	0.064	0.01	0.01	68.7	77.2

Table 4

Summary of TROPOMI/GRASP, VIIRS/DB and MODIS/TERRA DT + DB AOD 550 nm validation metrics with AERONET over four classes of land surface ($0 < NDVI \leq 0.2$, $0.2 < NDVI \leq 0.4$, $0.4 < NDVI \leq 0.6$, and $0.6 < NDVI \leq 1$). In each individual NDVI class, the best performing metric is indicated in bold.

NDVIs	Products (Num. Matchups)	R	Slope	Offset	RMSE	BIAS	BIAS _{AOD < 0.2}	GCOS (%)	Target (%)
$0 < NDVI \leq 0.2$	TROPOMI (366)	0.903	0.943	0.068	0.120	0.06	0.07	34.4	42.6
	VIIRS (435)	0.894	0.943	0.036	0.082	0.03	0.03	49.4	57.9
	MODIS (330)	0.807	0.708	0.034	0.121	-0.02	0.01	49.7	60.3
$0.2 < NDVI \leq 0.4$	TROPOMI (1760)	0.923	0.872	0.016	0.065	0.00	0.00	61.0	72.6
	VIIRS (1521)	0.880	0.814	0.014	0.070	-0.01	0.00	59.2	69.3
	MODIS (1076)	0.803	0.876	0.041	0.098	0.02	0.03	46.1	57.6
$0.4 < NDVI \leq 0.6$	TROPOMI (2401)	0.875	0.789	0.033	0.079	0.01	0.01	55.7	66.3
	VIIRS (2045)	0.926	1.058	0.002	0.083	0.01	0.01	61.6	71.5
	MODIS (2273)	0.939	1.077	0.006	0.098	0.02	0.01	54.9	67.0
$0.6 < NDVI \leq 1$	TROPOMI (672)	0.811	0.870	0.004	0.054	-0.01	0.00	67.3	76.8
	VIIRS (454)	0.776	0.769	0.015	0.072	-0.01	-0.01	79.1	86.8
	MODIS (656)	0.845	1.111	0.022	0.120	0.04	0.03	55.2	66.5

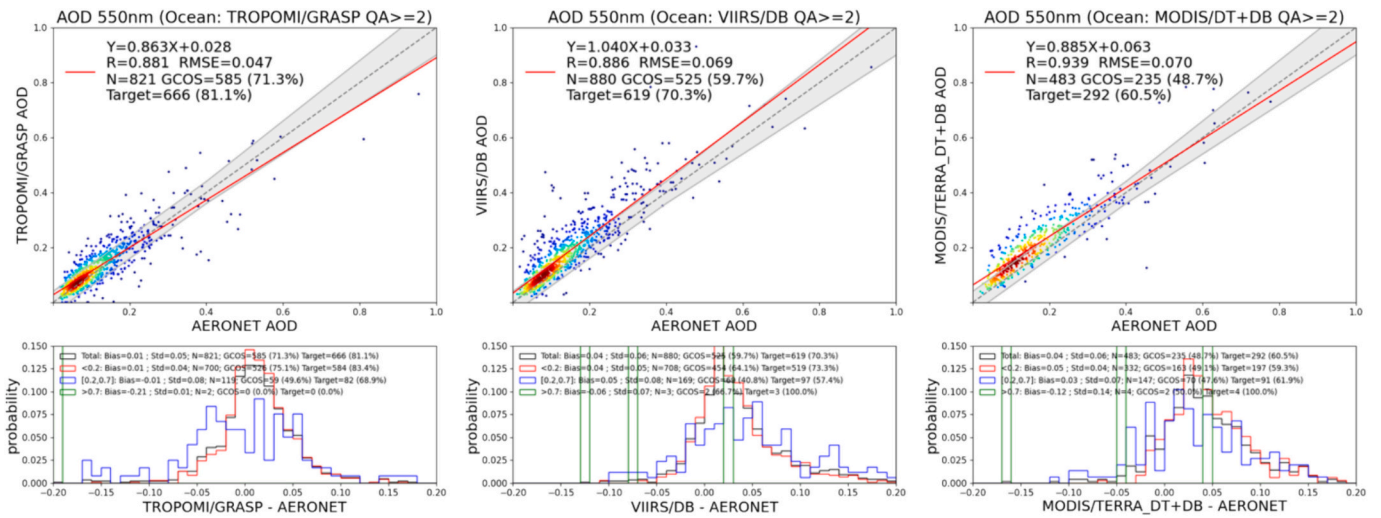


Fig. 2. The same as Fig. 1, but for AOD 550 nm validation over ocean.

MODIS/DT + DB AOD (550 nm) over ocean for one year period March 2019 to February 2020. Over ocean, MODIS/DT + DB AOD show the highest R (0.939) and all products with $R > 0.88$. Yet, MODIS/DT + DB combined AOD show a positive bias 0.04–0.05, which is consistent with the MODIS team validation (Remer et al., 2020). VIIRS/DB also show a positive bias around ~ 0.04 , while the GCOS and Target fractions of VIIRS/DB (59.7% GCOS and 70.3% Target) are higher than that of MODIS/DT + DB (48.7% GCOS and 60.5% Target). Moreover, TROPOMI/GRASP show excellent agreement with AERONET with the smallest RMSE (0.047) and the highest GCOS (71.3%) and Target (81.1%) fractions. In addition, the BIAS and BIAS_{AOD < 0.2} is within 0.01. As shown in Part I (Litvinov et al., 2024, Part I), the use of wind speed to constrain angular properties of ocean surface BRDF significantly improve the TROPOMI/GRASP aerosol retrieval, especially for the reduction of bias in AOD, which was also observed previously for OCLI/Sentinel-3 GRASP retrieval over ocean (Chen et al., 2022b). The

statistics for spectral AOD (490, 550 and 670 nm) validation over ocean are summarized in Table 5. Overall, the VIIRS/DB shows slightly better R and Slope than TROPOMI/GRASP, yet TROPOMI/GRASP has smaller RMSE, BIAS, BIAS_{AOD < 0.2} and higher GCOS and Target fractions. Spectrally, the TROPOMI/GRASP AOD is with BIAS not exceeding 0.02, RMSE smaller than 0.055, GCOS fraction higher than 64% and Target fraction higher than 75%.

3.1.2. Intercomparison of Ångström exponent (AE) products validation with AERONET

The Ångström exponent (AE) from TROPOMI/GRASP and VIIRS/DB are validated with AERONET and intercompared in this section. Even though AE is not provided in VIIRS/DB product, we calculate it using AODs at 2 channels: AE (412/670 nm) over land and AE (490/670 nm) over ocean. Meanwhile, TROPOMI/GRASP AE (412/670 nm) is validated over both land and ocean. Because the uncertainty of satellite

Table 5

Summary of TROPOMI/GRASP, VIIRS/DB and MODIS/TERRA DT + DB spectral AOD validation metrics with AERONET reference dataset over ocean. The best performing metric is indicated in bold.

Land/Ocean	Bands (nm)	Products (Num. Matchups)	R	Slope	Offset	RMSE	BIAS	BIAS _{AOD < 0.2}	GCOS (%)	Target (%)
Ocean	490	TROPOMI (821)	0.883	0.920	0.026	0.055	0.01	0.02	64.6	75.3
		VIIRS (880)	0.887	1.054	0.035	0.079	0.04	0.04	55.3	65.7
	550	TROPOMI (821)	0.881	0.863	0.028	0.047	0.01	0.01	71.3	81.1
		VIIRS (880)	0.886	1.040	0.033	0.069	0.04	0.04	59.7	70.3
	670	MODIS (483)	0.939	0.885	0.063	0.070	0.04	0.05	48.7	60.5
		TROPOMI (821)	0.869	0.740	0.029	0.040	0.00	0.01	81.7	89.0
		VIIRS (880)	0.876	1.001	0.035	0.058	0.03	0.03	65.0	74.3

derived AE strongly rely on the aerosol loading, particularly a small error of AOD at different wavelengths could have a huge effect on calculated AE especially when AOD is low (Chen et al., 2020). TROPOMI/GRASP provides quality flag (QAExtend) for such extended properties. As suggested in Part I (Litvinov et al., 2024), we use the highest QAExtend = 3 over land and QAExtend \geq 2 to select TROPOMI/GRASP AE (412/670 nm) for validation. For VIIRS/DB, we select QA \geq 2 with additional AOD (550 nm) > 0.2 over land and QA \geq 2 over ocean.

Fig. 3 shows the validation of TROPOMI/GRASP AE (412/670 nm) and VIIRS/DB AE (land: 412/670 nm; ocean: 490/670 nm) over land and ocean with AERONET for an entire year (March 2019 to February 2020). The fractions of retrievals within the AE Optimal (+/- 0.3) and Target (+/- 0.5) are also present in the figure. Over land, TROPOMI/GRASP show convincing capability to separate two groups with fine (AE > 1) and coarse (AE < 1) particles, despite the AE is slightly overestimated for both fine and coarse particles that is known issue for GRASP/Models approach (Chen et al., 2020, 2022b). In contrast, VIIRS/DB AE is less convincing in identifying fine/coarse dominant cases, that is largely due to the use of region-specific aerosol models in the look-up-tables (LUT). Over ocean, TROPOMI/GRASP show similar pattern as the one over land that AE is overestimated generally, especially for coarse mode. Compared to TROPOMI/GRASP, VIIRS/DB AE show better correspondence with AERONET with R 0.62 and Optimal fraction 65.3%. It implies the general capability to derive aerosol size related information, such as AE, from single viewing radiometers over ocean.

3.1.3. Intercomparison of AODF and AODC products validation with AERONET

The validations of TROPOMI/GRASP and VIIRS/DB AODF and AODC at 550 nm over ocean surface with AERONET Version 3 Level 2 SDA product are intercompared in this section. The DT algorithm provides MODIS AODF and AODC over ocean, which is not included in the intercomparison. TROPOMI/GRASP provides AODF and AODC at 10 wavelengths over land and ocean, and the validation for different QA index is present in Part I (Litvinov et al., 2024). For VIIRS/DB product, the fine mode fraction (FMF) at 550 nm is used to derive AODF and AODC at 550 nm together with AOD (550 nm). Due to the VIIRS/DB AODF and AODC only available at 550 nm over ocean, in this section we will intercompare the validation results over ocean. AERONET SDA fine/coarse mode AOD (τ_f and τ_c) is provided at 500 nm along with the fine mode Ångström exponent (α_f), therefore the interpolation into 550 nm can be done as:

$$\tau_f(550 \text{ nm}) = \tau_f(500 \text{ nm}) * (550/500)^{-\alpha_f} \quad (1)$$

$$\tau_c(550 \text{ nm}) = \tau(550 \text{ nm}) - \tau_f(550 \text{ nm}) \quad (2)$$

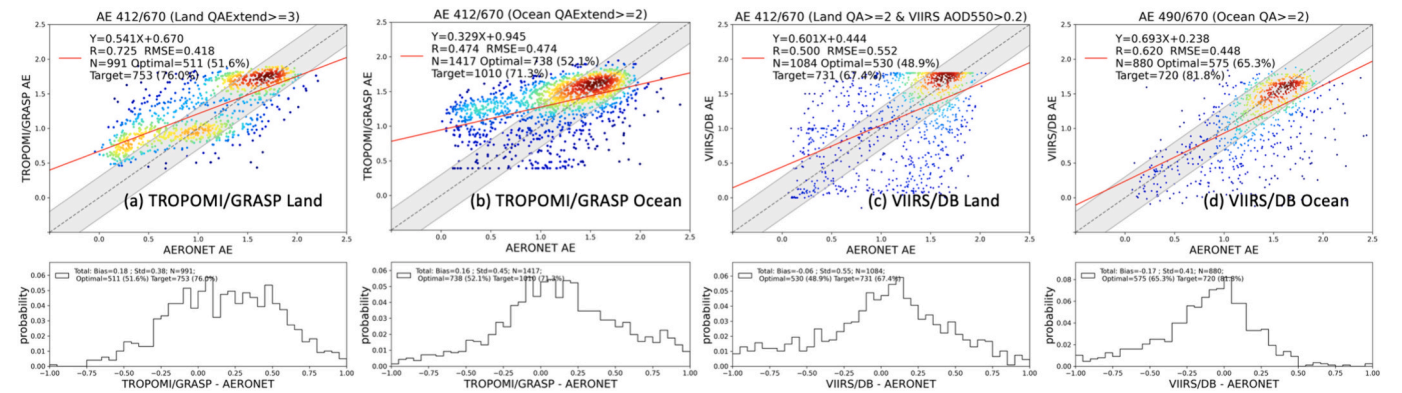


Fig. 3. Validation of TROPOMI/GRASP and VIIRS/DB AE over land and ocean with AERONET for an entire year (March 2019 to February 2020). The gray dashed line and the red solid line are the 1:1 reference line and the linear regression line. The gray envelope indicates Optimal requirement for AE (+/- 0.3). The percentage of retrievals satisfying the Target requirement for AE (+/- 0.5) and the probability density function of differences between satellite and AERONET AE are also presented in the lower panels. (For interpretation of the references to colour in this figure legend, the reader is referred to the web version of this article.)

Fig. 4 shows the TROPOMI/GRASP and VIIRS/DB AODF (550 nm) validation over ocean. We continue to calculate the GCOS - max (0.04 or 10%AODF) and Target - max (0.05 or 20%AODF) fractions for AODF and AODC validations (Litvinov et al., 2024). To be consistent with the AOD validation over ocean, the QA \geq 2 is used for both products to select high quality retrievals. Generally, TROPOMI/GRASP and VIIRS/DB AODF (550 nm) show similar performance against AERONET SDA over ocean: TROPOMI/GRASP (R = 0.816, RMSE = 0.040, BIAS = 0.01 and $\text{BIAS}_{\text{AODF} < 0.2} = 0.01$) and VIIRS/DB (R = 0.807, RMSE = 0.046, BIAS = 0.01 and $\text{BIAS}_{\text{AODF} < 0.2} = 0.01$). Moreover, the GCOS and Target fractions are also comparable, that \sim 80% satisfying GCOS requirement and \sim 85% satisfying Target requirement for both products.

The AODC (550 nm) validation of TROPOMI/GRASP and VIIRS/DB over ocean with AERONET is present in Fig. 5. Generally, the agreement between TROPOMI/GRASP and VIIRS/DB AODC (550 nm) with AERONET over ocean is less good than that of AODF. The correlation coefficient (R) is around 0.8 for 2 products. While VIIRS/DB shows evident overestimation \sim 0.04–0.06, which explains that the positive bias (\sim 0.04) of VIIRS/DB AOD (550 nm) over ocean is mainly from the overestimation of the coarse mode contribution. TROPOMI/GRASP AODC (550 nm) has good agreement with AERONET when AODC is lower than 0.2 where \sim 93% retrievals satisfy the GCOS requirement and the $\text{BIAS}_{\text{AODC} < 0.2}$ is around 0.01. While TROPOMI/GRASP tends to underestimate AODC when the AODC loading increases, for example, the $\text{BIAS}_{0.2 < \text{AODC} \leq 0.7}$ is -0.17. This explains that TROPOMI/GRASP underestimates AOD (550 nm) over ocean when aerosol loading is high (Fig. 2).

3.1.4. Intercomparison of SSA products validation with AERONET

Even though spectral SSA is not the main product, it is still diagnosed in the VIIRS/DB L2 product over land at 412, 490 and 670 nm. The TROPOMI measurements at UV provide the sensitivity to the aerosol absorption, therefore, the GRASP algorithm derives TROPOMI SSA at 10 wavelengths (Litvinov et al., 2024). The validation of TROPOMI/GRASP spectral SSA at different QAExtend index is present in Part I (Litvinov et al., 2024). Here we intercompare the validation metrics at the 3 common wavelengths (412, 490 and 670 nm). The matchup methodology between satellite retrievals and AERONET Level 2 inversion product uses a larger time window (+/- 180 mins) than the matchup with AERONET direct-sun measurements due to the relative rare AERONET sky radiance measurements that is used to derive inversion products, including size distribution, spectral SSA, spectral aerosol absorption optical depth (AAOD or τ_a), complex refractive index, fraction of spherical particles (Dubovik and King, 2000; Dubovik et al., 2000, 2006). In addition, the TROPOMI/GRASP quality flag for extended properties (QAExtend = 3) is used to select high quality TROPOMI/

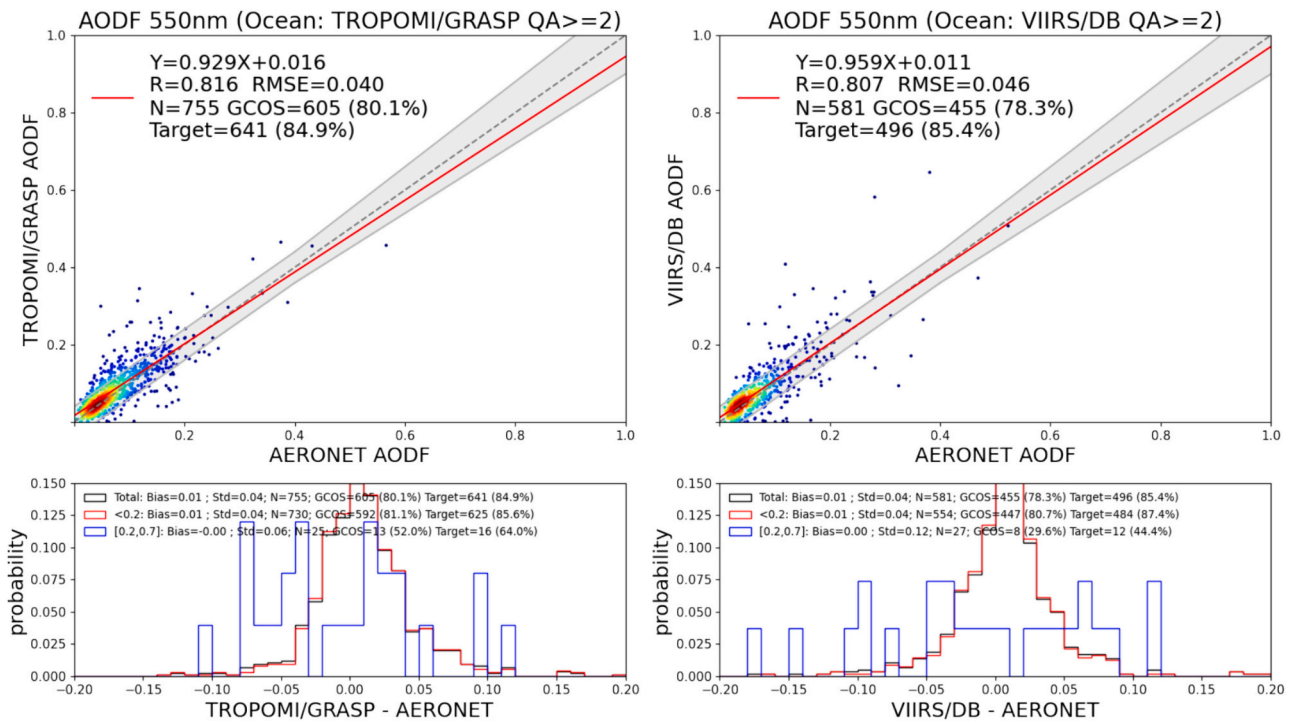


Fig. 4. Validation of TROPOMI/GRASP and VIIRS/DB AODF 550 nm over ocean with AERONET for an entire year (March 2019 to February 2020). The gray dashed line and the red solid line are the 1:1 reference line and the linear regression line. The gray envelope indicates GCOS requirement for AODF (max 0.04 or 10% AODF). The probability density function of differences between satellite and AERONET AODF and the Bias under different AODF conditions (any AODF, AODF<0.2, 0.2 ≤ AODF≤0.7 and AODF>0.7) are present in the lower panels. (For interpretation of the references to colour in this figure legend, the reader is referred to the web version of this article.)

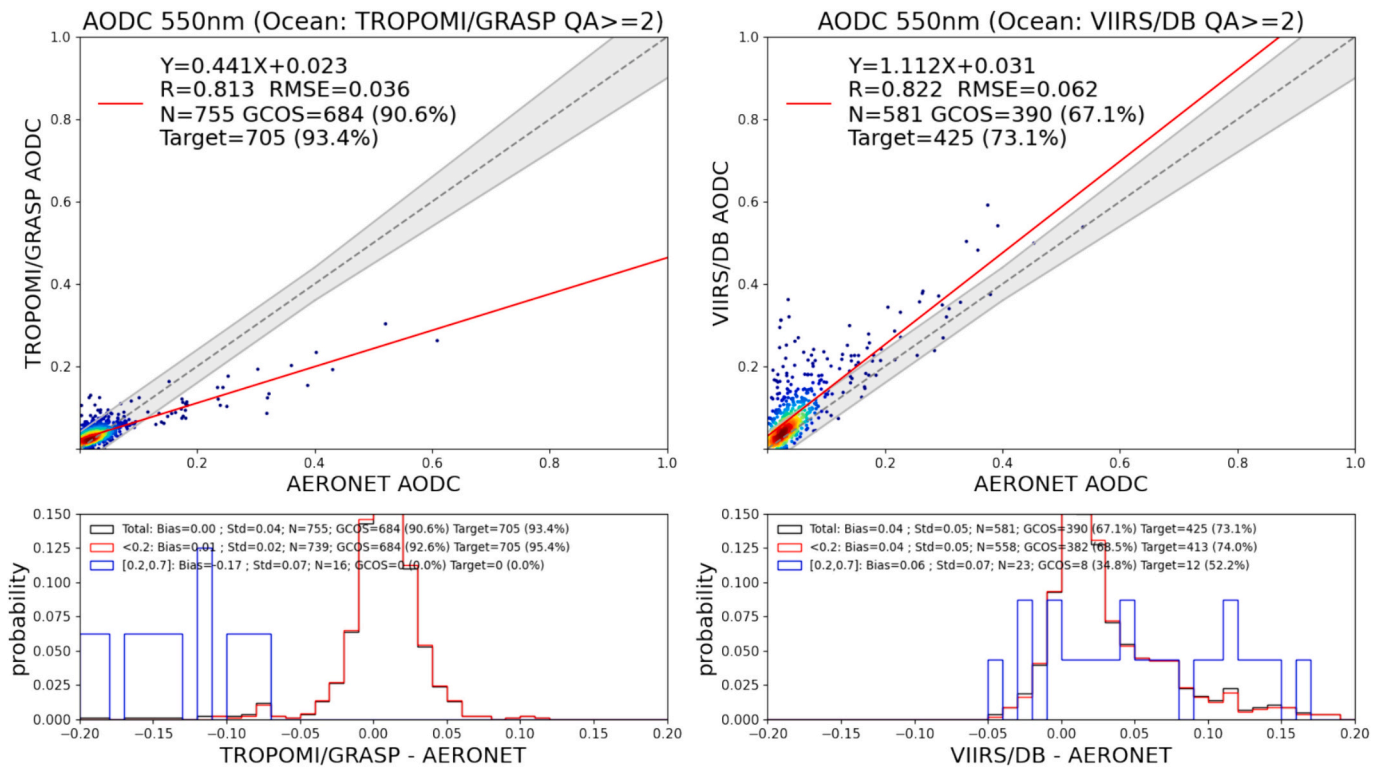


Fig. 5. The same as Fig. 4, but for AODC 550 nm validation over ocean.

GRASP SSA products (Litvinov et al., 2024). Since AERONET SSA products are available at 440, 675, 870 and 1020 nm, we interpolate and extrapolate using absorption Ångström exponent ($\alpha_a = \frac{\ln\tau_a(\lambda_2) - \ln\tau_a(\lambda_1)}{\ln\lambda_1 - \ln\lambda_2}$, where λ represent wavelength and τ_a is AAOD). For example, the interpolation of AERONET SSA (ω) into 490 nm can be done through Eqs. 3–5 using $\alpha(440\text{--}870\text{ nm})$ and $\alpha_a(440\text{--}870\text{ nm})$:

$$\tau_a(490\text{ nm}) = \tau_a(440\text{ nm}) * (490/440)^{-\alpha_a} \quad (3)$$

$$\tau(490\text{ nm}) = \tau(440\text{ nm}) * (490/440)^{-\alpha} \quad (4)$$

$$\omega(490\text{ nm}) = 1 - \tau_a(490\text{ nm})/\tau(490\text{ nm}) \quad (5)$$

Fig. 6 shows the validation of TROPOMI/GRASP and VIIRS/DB SSA (490 nm) over land with AERONET for an entire year. The validation metrics for 3 wavelengths (412, 490 and 670 nm) are summarized in Table 6. We calculate the retrievals satisfying the Optimal and Target requirements for SSA that are ± 0.03 for Optimal and ± 0.05 for Target requirements (Litvinov et al., 2024). Generally, TROPOMI/GRASP SSA shows better agreement with AERONET than VIIRS/DB, for example, at 490 nm the R is 0.478 with RMSE 0.026 for TROPOMI/GRASP in contrast with VIIRS/DB R = -0.489 and RMSE 0.058. For TROPOMI/GRASP spectral SSA, at least 75% of them fit the Optimal requirement and at least 89% is within Target requirement, which are superior to VIIRS/DB SSA of at least 39% and 57% retrievals satisfying Optimal and Target requirements.

3.2. Intercomparison of validation of surface products with S5P/TROPOMI surface reference dataset

Here we present the results of the intercomparison of validation of surface products S5P/TROPOMI GRASP and MODIS (TERRA+AQUA) monthly surface products as well as OMI, GOME-2 and SCIAMACHY

surface LER climatology with the surface reference dataset over 30 selected AERONET sites generated from the GROSAT S5P/TROPOMI and AERONET combined retrieval (Litvinov et al., 2020; Litvinov et al., 2022). The validation is performed for all available common bands. The difference of the center wavelength not exceeding 20 nm is considered as a common band. Due to the fact that the surface normally does not change rapidly, the validation therefore is performed using TROPOMI/GRASP and MODIS monthly mean and climatological mean for OMI, GOME-2 and SCIAMACHY. MODIS MCD43 surface product is based on the accumulation of 16-days TERRA + AQUA data and weighted to the day of interest, therefore, we simply use the 15th day of each month to represent the MODIS monthly mean. The GROSAT reference dataset provides $3 \times 3 \times 10\text{ km}$ pixels over 30 selected AERONET sites. Therefore, the nearest MODIS MCD43 0.05 degree pixels (MODIS 0.05° center coordinates nearest to the TROPOMI 10 km center coordinates) are used for validation, and the exact corresponding TROPOMI/GRASP 10 km pixels are selected for validation since TROPOMI/GRASP and GROSAT are produced on the same grids. For OMI, GOME-2 and SCIAMACHY surface LER, we re-grid GROSAT reference dataset provided $3 \times 3 \times 10\text{ km}$ pixels into one single pixel to validate with corresponding OMI and GOME-2 0.25° grid boxes and SCIAMACHY 0.5° grid boxes. Specifically, the GROSAT $3 \times 3 \times 10\text{ km}$ pixels are averaged to compare with the nearest OMI, GOME-2 0.25° and SCIAMACHY 0.5° grid boxes. We would like to emphasize that surface inhomogeneity could play a vital role and potential impart the performed intercomparison due to the differences in pixel footprints and re-grided boxes of each satellite product.

Fig. 7 shows the validation of (a) TROPOMI/GRASP and (b) MODIS/MCD43C3 white sky albedo (BHR_ISO) with S5P/TROPOMI surface reference dataset over 30 AERONET stations over one year period. The validation of (c) SCIAMACHY, (d) OMI and (e) GOME-2 climatological LER with S5P/TROPOMI surface reference BHR_ISO are present in Fig. 7c-e. We calculate the percentage of retrievals satisfying both

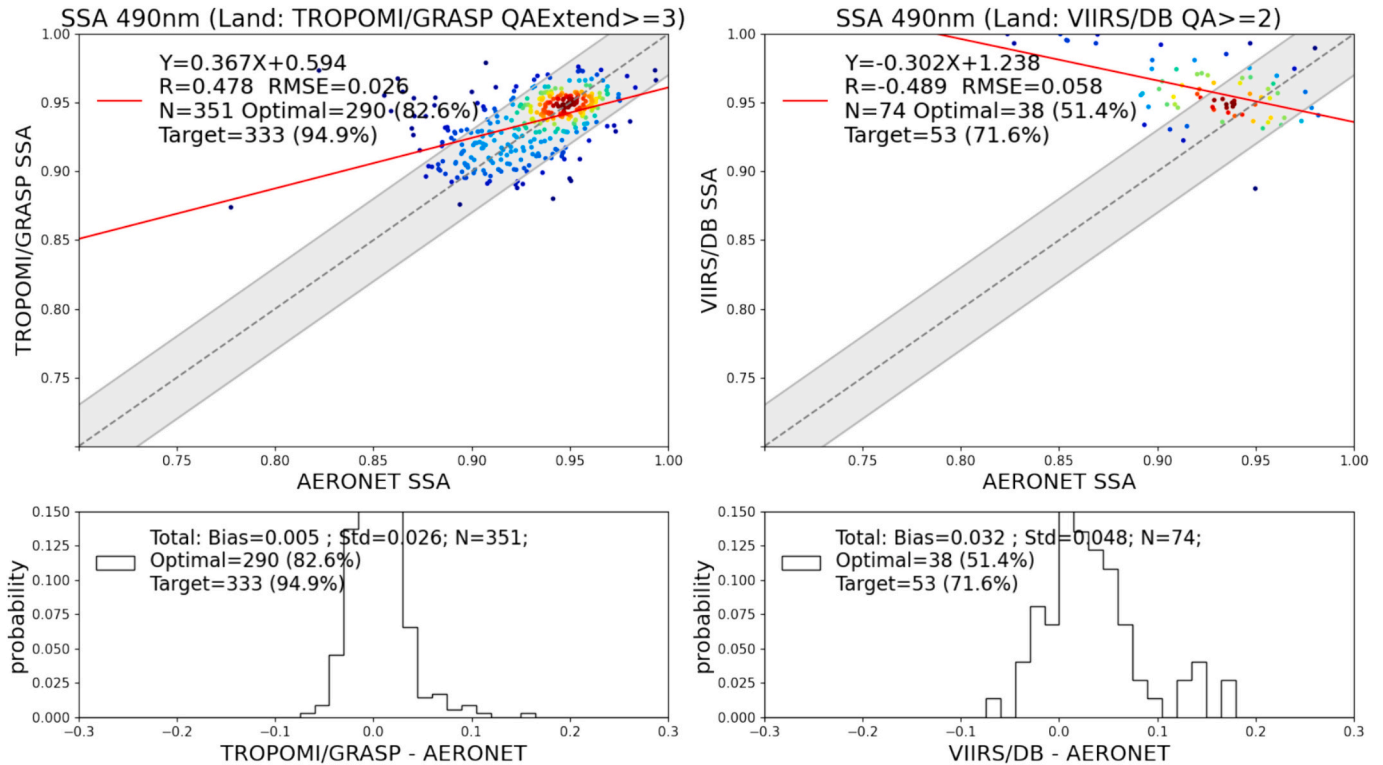


Fig. 6. Validation of TROPOMI/GRASP and VIIRS/DB SSA 490 nm over land with AERONET for an entire year (March 2019 to February 2020). The gray dashed line and the red solid line are the 1:1 reference line and the linear regression line. The gray envelope indicates Optimal requirement for SSA (± 0.03). The percentage of retrievals satisfying the Target requirement for SSA (± 0.05) and the probability density function of differences between satellite and AERONET SSA are also present. (For interpretation of the references to colour in this figure legend, the reader is referred to the web version of this article.)

Table 6

Summary of TROPOMI/GRASP and VIIRS spectral SSA validation metrics with AERONET reference dataset over land. The best performing metric is indicated in bold.

Land/Ocean	Products (Num. Matchups)	Bands (nm)	R	RMSE	BIAS	Optimal +/- 0.03 (%)	Target +/- 0.05 (%)
Land	VIIRS/DB (74)	412	-0.360	0.064	0.034	39.2	56.8
		490	-0.489	0.058	0.032	51.4	71.6
		670	-0.137	0.069	0.037	63.5	71.6
	TROPOMI/GRASP (351)	412	0.452	0.031	0.011	75.8	90.9
		490	0.478	0.026	0.005	82.6	94.9
		670	0.673	0.035	0.010	74.6	88.9

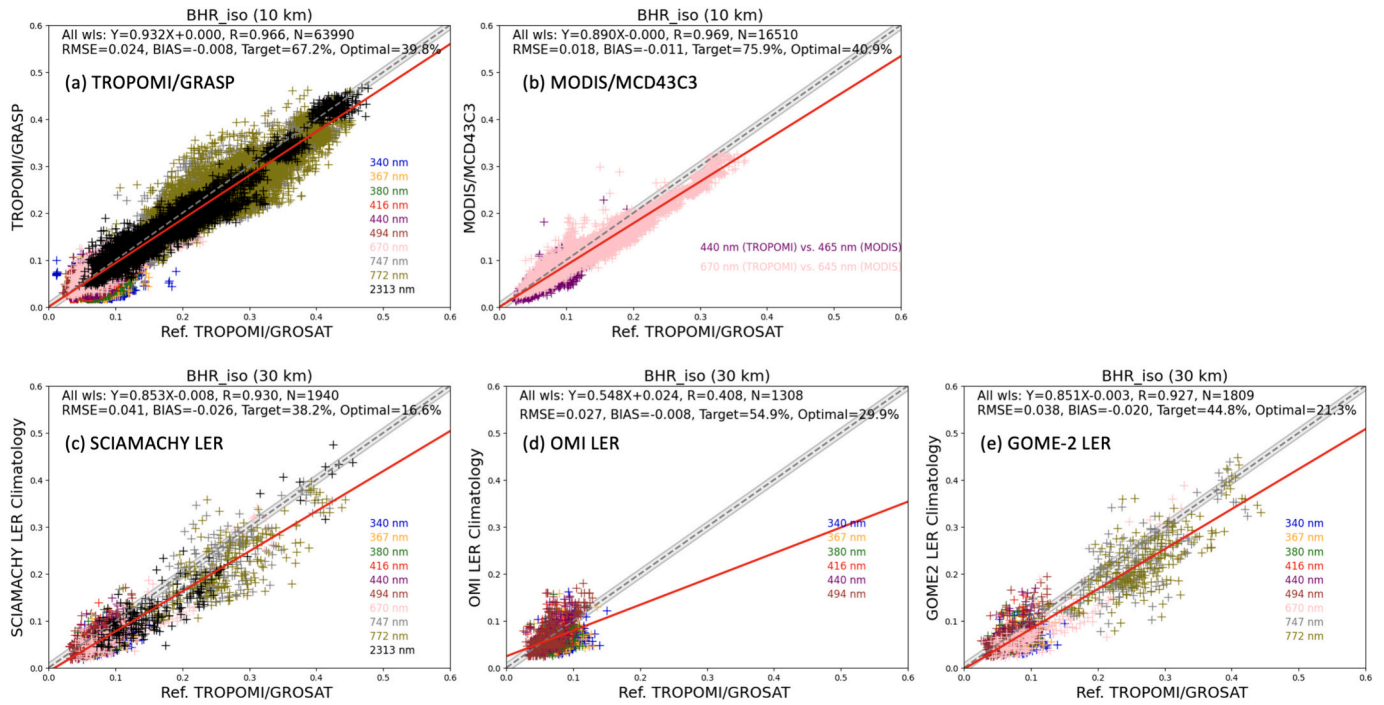


Fig. 7. Validation of (a) TROPOMI/GRASP and (b) MODIS/MCD43C3 white sky albedo (or BHR_ISO) with S5P/TROPOMI surface reference dataset. The validation of (c) SCIAMACHY, (d) OMI and (e) GOME-2 climatological LER with S5P/TROPOMI surface reference BHR_ISO are also present. The gray dashed line and the red solid line are the 1:1 reference line and the linear regression line. The gray envelope indicates Target requirement for surface. The statistical metrics for each corresponding wavelength are shown in the Appendix Tables A1-A5. (For interpretation of the references to colour in this figure legend, the reader is referred to the web version of this article.)

Optimal and Target requirements for surface validation. The formulated surface Optimal (+/- 0.01) and Target (+/- 0.02) requirements are present in Part I Table 1 (Litvinov et al., 2024). The linear fitting correlation coefficient R, Slope and Offset are calculated for combined all common wavelengths, and the Optimal and Target fractions, RMSE and BIAS are calculated for each common wavelength as well as for all combined wavelengths, and the statistical metrics are shown in the Appendix Tables A1-A5. Since the common wavelengths are different from dataset to dataset, the dynamic range varies which affects the calculation of R for the combined all wavelengths. Generally, the surface products are in better agreement with the reference dataset at VIS than UV, NIR and SWIR. Moreover, the surface products tend to underestimate surface albedo (BHR_ISO) at UV, NIR and SWIR. For example, the BIAS is around -0.01 to -0.03 at UV, and it decreases to nearly zeros (within 0.01) at 440 to 490 nm, and starting from 670 nm to SWIR (2313 nm) the BIAS is around -0.01 to -0.05. The dispersion (RMSE) between SCIAMACHY, OMI and GOME-2 climatological LER and S5P/TROPOMI surface reference is generally higher than that between TROPOMI and MODIS with the GROSAT surface reference. For example, the RMSEs at 440 nm blue channel are 0.018 (TROPOMI/GRASP), 0.016 (MODIS/MCD43C3), 0.022 (SCIAMACHY), 0.022 (OMI) and 0.022 (GOME-2). Even though the BIAS for each product is smaller than 0.01 except for SCIAMACHY (0.011). We should consider the fact that the

SCIAMACHY, OMI and GOME-2 climatology are generated based on several years of data. Moreover, the climatological datasets are of coarser spatial resolution than MODIS and TROPOMI. These factors may induce some uncertainties. Furthermore, we should note the discrepancy at the red channel (670 nm). Although all available products tend to underestimate at 670 nm, the BIAS for TROPOMI and MODIS is around -0.006 to -0.01, which is 3-5 times smaller than that of SCIAMACHY (-0.030) and GOME-2 (-0.028). The Optimal fraction is around 45% for TROPOMI and MODIS in contrast around 15% for SCIAMACHY and GOME-2.

4. Global intercomparison of aerosol and surface products

The aerosol and surface products are validated and intercompared with reference datasets in section 3. In this section, we will re-grid all the aerosol and surface products into a common grid and intercompare at pixel/grid level for one entire year. Specifically, we make pixel-to-pixel intercomparison between S5P/TROPOMI GRASP, Suomi-NPP/VIIRS DB and MODIS/TERRA DT + DB aerosol products globally. The monthly S5P/TROPOMI GRASP, MODIS MCD43 surface products together with OMI, GOME-2 and SCIAMACHY surface LER monthly climatology are also intercompared for one entire year.

4.1. Aerosol products intercomparison

4.1.1. AOD products intercomparison

Due to the different spatial resolution of the aerosol products, e.g. 10 km TROPOMI/GRASP, 6 km VIIRS/DB at nadir and ~ 10 km near the edges of the swath and 10 km MODIS/DT + DB at nadir and ~ 50 km near the edges, we re-grid the 3 products into a common 0.2° grid box under equirectangular projection and intercompare the aerosol products at the 0.2° grid box globally. To assure the quality of the retrieval products for re-gridding, we keep using the same QA flag to select the products as for validation in section 3 that are $QA \geq 2$ for all products over ocean, and $QA = 3$ for TROPOMI/GRASP and MODIS/DT + DB products and $QA \geq 2$ for VIIRS/DB over land. Fig. 8 shows the spatial distribution of one-year (March 2019 – February 2020) AOD 550 nm from independent TROPOMI/GRASP, VIIRS/DB and MODIS/DT + DB products. The 0.2° pixel level difference of AOD 550 nm averaged over a year is presented as VIIRS/DB – TROPOMI/GRASP and MODIS/DT + DB – TROPOMI/GRASP. Note that the differences are calculated for common pixels and then averaged for a year, and we require the minimal occupancy of 10 over a year to calculate the mean differences between products. The pixel-to-pixel statistic metrics for spectral AOD are listed in Table 7. The statistic metrics are estimated using linear regression model (ordinary least squares). The PDF for AOD (550 nm) differences over land and ocean are present in Fig. 9a-b.

Over ocean, although the validation with AERONET coastal sites (Fig. 2-Validation) shows VIIRS/DB AOD 550 nm is off by $+0.04$ and the BIAS is $+0.01$ for TROPOMI/GRASP, TROPOMI/GRASP and VIIRS/DB

AOD show overall excellent consistency. The difference for AOD 550 nm (VIIRS - TROPOMI) is -0.002 ($1\sigma = 0.033$), and the pixel-to-pixel R is 0.959 with RMSE 0.033 for >10 million matchup pixels (10802353), and 85.7% of them satisfying GCOS uncertainty requirement and 92.4% of them satisfying Target requirement. In addition, the agreement remains for other common wavelengths (490 and 670 nm). For example, the R is higher than 0.95 and RMSE smaller than 0.05 for all 3 common wavelengths (490, 550, and 670 nm). The differences (VIIRS - TROPOMI) are -0.011 for AOD at 490 nm and $+0.013$ at 670 nm. On the other hand, MODIS/TERRA show slightly higher AOD at 550 nm than TROPOMI/GRASP as well as VIIRS/DB over ocean. This is consistent with the AERONET coastal sites validation (Fig. 2-Validation) and validation from the MODIS team that show a positive bias around 0.04–0.05 for MODIS/TERRA AOD over ocean. The global pixel-to-pixel difference based on ~ 10 million pairs between MODIS/TERRA and TROPOMI AOD (550 nm) over ocean is 0.014 ($1\sigma = 0.088$), and the standard deviation $1\sigma = 0.088$ is about 2.5 times larger than that between VIIRS and TROPOMI with $1\sigma = 0.033$, which leads to relatively lower fractions for GCOS (59.3%) and Target (69.2%). Overall, over ocean the agreement between 2 independent sensors (TROPOMI and VIIRS) and algorithms (GRASP and DB) is very good according to all statistical characteristics and applied requirements.

Over land, the discrepancy between products is much higher than that over ocean, which is well known problem caused by the general complexity of aerosol retrieval over land surfaces. Generally, TROPOMI/GRASP tends to report lower AOD over high latitude areas (such as Siberia and Canada) and higher AOD over Taklimakan desert and its

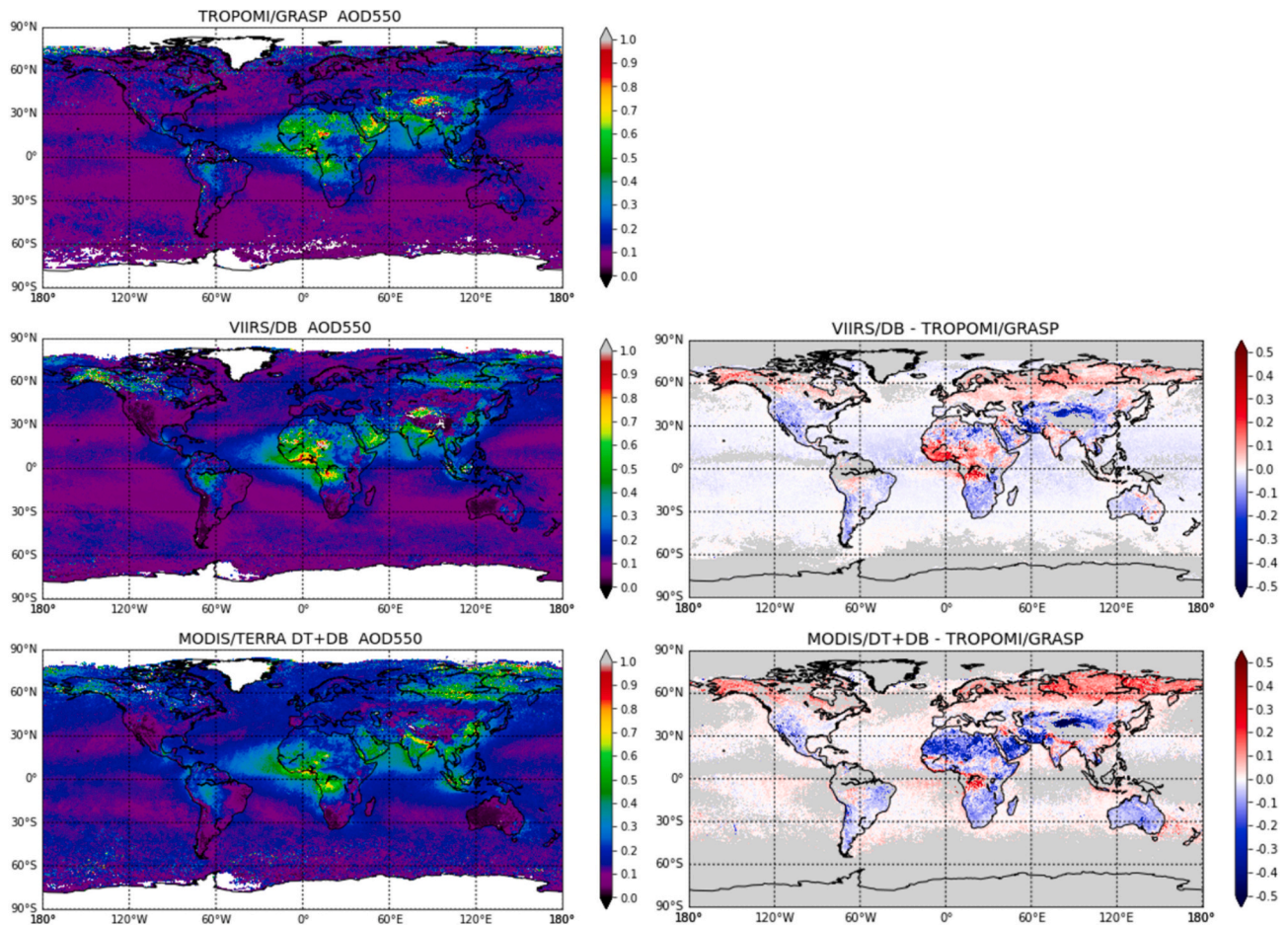


Fig. 8. Spatial distribution of one-year (March 2019 – February 2020) AOD 550 nm from TROPOMI/GRASP, VIIRS/DB and MODIS/TERRA DT + DB products. The pixel level difference of AOD 550 nm averaged over a year is presented as VIIRS/DB – TROPOMI/GRASP and MODIS/TERRA DT + DB – TROPOMI/GRASP. Note only the pixels with appearances $N \geq 10$ during a year are accounted for in the difference calculation.

Table 7

Summary of global pixel-to-pixel spectral AOD statistic metrics between VIIRS/DB, MODIS/TERRA DT + DB and TROPOMI/GRASP over land and ocean.

Land/Ocean	Products (Num. Matchups)	Bands (nm)	R	Slope	Offset	RMSE	Diff. (MODIS or VIIRS - TROPOMI)	GCOS (%)	Target (%)	
Land	VIIRS vs. TROPOMI (10626593)	412	0.873	0.876	0.007	0.136	-0.021	35.3	46.0	
		490	0.877	0.927	0.006	0.111	-0.007	42.0	52.9	
		550	0.881	0.957	0.005	0.100	-0.002	46.5	57.2	
		670	0.871	1.049	0.003	0.094	0.009	54.6	64.3	
Ocean	MODIS vs. TROPOMI (8204323)	550	0.757	0.712	0.020	0.144	-0.032	36.4	45.8	
		VIIRS vs. TROPOMI (10802353)	490	0.950	0.845	0.011	0.045	-0.011	77.3	86.1
			550	0.957	0.900	0.010	0.033	-0.002	85.7	92.4
			670	0.959	1.034	0.010	0.028	0.013	87.9	93.3
MODIS vs. TROPOMI (9057816)	550	0.748	0.733	0.052	0.089	0.014	59.3	69.2		

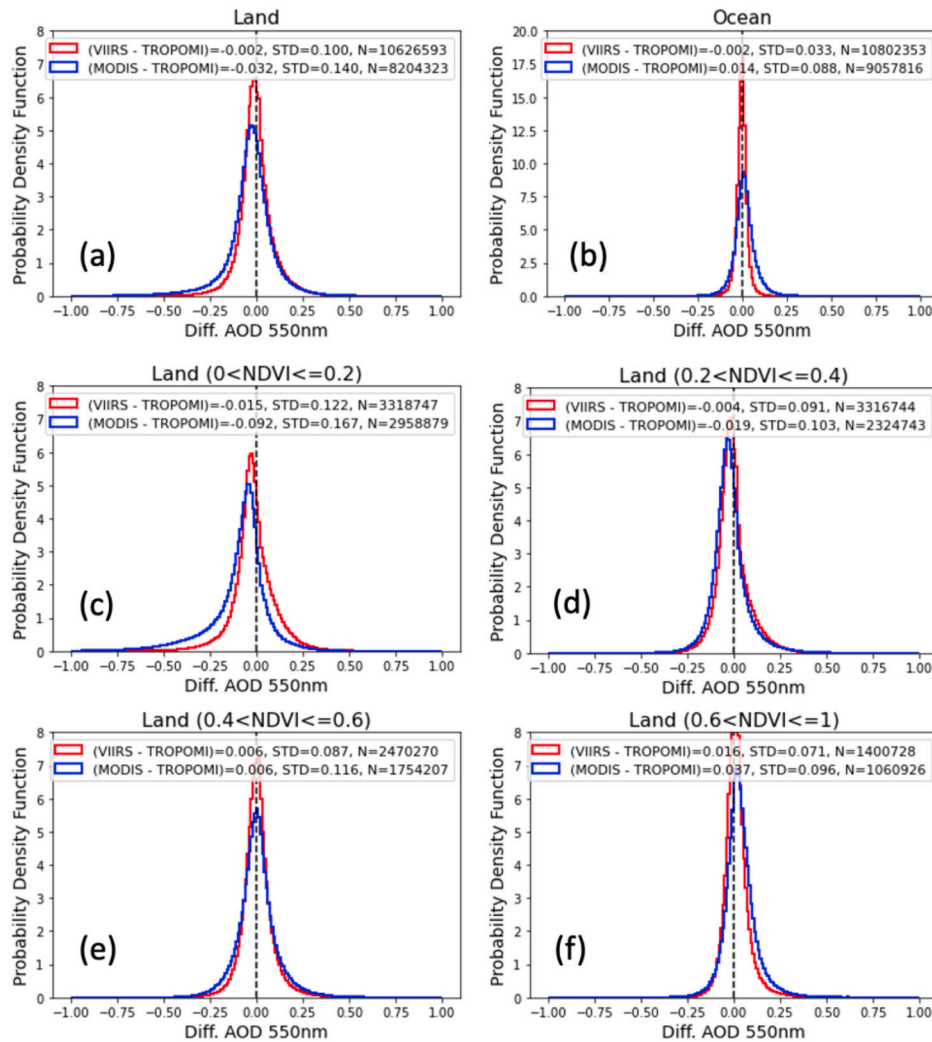


Fig. 9. Possibility density function (PDF) of pixel level AOD (550 nm) differences between VIIRS/DB, MODIS/TERRA DT + DB and TROPOMI/GRASP over (a) land and (b) ocean, as well as the PDF split for different land surface NDVIs: (c) $0 < NDVI \leq 0.2$, (d) $0.2 < NDVI \leq 0.4$, (e) $0.4 < NDVI \leq 0.6$, (f) $0.6 < NDVI \leq 1$.

downwind northwestern China than VIIRS/DB and MODIS/TERRA DT + DB. Over north Africa Sahara Desert, the MODIS/TERRA is evidently lower than TROPOMI and VIIRS. All 3 AOD products show high aerosol loading over equatorial Africa, while the spatial distribution is slightly different that MODIS/TERRA and VIIRS tend to be higher than TROPOMI in the southern part and VIIRS is higher than MODIS/TERRA and TROPOMI in the northern part. Based on 10,626,593 pixels between VIIRS and TROPOMI over land, the difference (VIIRS - TROPOMI) of AOD (550 nm) is -0.002 ($1\sigma = 0.1$). Statistically, the difference between MODIS and TROPOMI (MODIS - TROPOMI) is -0.034 ($1\sigma = 0.14$) which is larger than the difference (VIIRS - TROPOMI). In addition, the pixel-

to-pixel agreement between VIIRS and TROPOMI ($R = 0.881$, $RMSE = 0.100$, $GCOS = 46.5\%$) is also better than MODIS and TROPOMI ($R = 0.757$, $RMSE = 0.144$, $GCOS = 36.4\%$). The TROPOMI/GRASP and VIIRS/DB AOD show good agreement spectrally from deep blue (412 nm) to red (670 nm) channels with R higher than 0.87 and RMSE smaller than 0.14. The AOD differences (VIIRS - TROPOMI) are smaller than ± 0.01 between 490 nm to 670 nm, and it increases to around -0.021 at 412 nm.

In order to investigate the AOD over different land surfaces, the further analysis of the pixel-to-pixel AOD between the 3 products was performed by splitting over 4 different land surface NDVIs (see in

Table 8

Summary of global pixel-to-pixel AOD 550 nm statistic metrics between TROPOMI/GRASP, VIIRS/DB and MODIS/TERRA DT + DB over four classes of land surface ($0 < \text{NDVI} \leq 0.2$, $0.2 < \text{NDVI} \leq 0.4$, $0.4 < \text{NDVI} \leq 0.6$, and $0.6 < \text{NDVI} \leq 1$).

NDVIs	Products (Num. Matchups)	R	Slope	Offset	RMSE	Diff. (MODIS or VII-S - TROPOMI)	GCOS (%)	Target (%)
$0 < \text{NDVI} \leq 0.2$	VIIRS vs. TROPOMI (3318747)	0.873	0.897	0.007	0.123	-0.015	38.1	49.6
	MODIS vs. TROPOMI (2958879)	0.749	0.566	0.015	0.191	-0.092	27.8	36.5
$0.2 < \text{NDVI} \leq 0.4$	VIIRS vs. TROPOMI (3316744)	0.853	1.026	-0.007	0.091	-0.004	46.4	56.0
	MODIS vs. TROPOMI (2324743)	0.804	0.991	-0.018	0.105	-0.019	40.0	49.5
$0.4 < \text{NDVI} \leq 0.6$	VIIRS vs. TROPOMI (2470270)	0.901	1.034	0.000	0.088	0.006	50.8	61.9
	MODIS vs. TROPOMI (1754207)	0.838	0.961	0.012	0.116	0.006	41.1	51.2
$0.6 < \text{NDVI} \leq 1.0$	VIIRS vs. TROPOMI (1400728)	0.928	1.069	0.008	0.072	0.016	58.6	69.3
	MODIS vs. TROPOMI (1060926)	0.887	1.077	0.027	0.103	0.037	44.7	54.8

Table 8): $0 < \text{NDVI} \leq 0.2$, $0.2 < \text{NDVI} \leq 0.4$, $0.4 < \text{NDVI} \leq 0.6$, and $0.6 < \text{NDVI} \leq 1$. We observe huge difference between MODIS and TROPOMI over bright surface ($0 < \text{NDVI} \leq 0.2$), where the pixel-to-pixel AOD (550 nm) difference is -0.092 ($1\sigma = 0.167$), and R is 0.749 with RMSE 0.191. VIIRS also shows smaller AOD than TROPOMI, while the difference is much smaller at -0.015 ($1\sigma = 0.122$), and the pixel-to-pixel R is 0.873 and RMSE is 0.123. For $0.2 < \text{NDVI} \leq 0.4$ area, the R between products is generally higher than 0.8 (0.853 for VIIRS and TROPOMI; 0.804 for MODIS and TROPOMI). The AOD (550 nm) difference between VIIRS and TROPOMI is -0.004 ($1\sigma = 0.091$), and -0.019 ($1\sigma = 0.103$) for MODIS and TROPOMI. For areas of $0.4 < \text{NDVI} \leq 0.6$, the AOD (550 nm) differences between MODIS, VIIRS and TROPOMI are the smallest among four different land surfaces. Both VIIRS and MODIS AOD 550 nm tend to be higher than TROPOMI about 0.006, and 1σ equals 0.087 for VIIRS and 0.116 for MODIS. For areas with dense vegetation ($0.6 < \text{NDVI} \leq 1$), the correlation coefficients R between MODIS, VIIRS and TROPOMI are higher than 0.88 which are the best among the four land surfaces. Overall, the TROPOMI/GRASP AOD seems to have generally better agreement with VIIRS/DB than with MODIS/TERRA DT + DB over all four types of land surfaces with higher correlation coefficient and smaller differences as well as higher GCOS and Target fractions.

4.1.2. AE products intercomparison

Both TROPOMI/GRASP and VIIRS/DB AOD products cover the spectral range 490 nm to 670 nm over land and ocean. The global pixel-to-pixel AE (490/670) between TROPOMI/GRASP and VIIRS/DB are performed in this section. First of all, the quality filter is consistent with that used in the validation section 3.1.2. In particular, $\text{QA}_{\text{Extend}} \geq 2$ and $\text{QA} \geq 2$ are used for TROPOMI/GRASP and VIIRS/DB respectively. The quality assured retrievals are then re-grid to common 0.2° grid boxes, and then the global pixel-to-pixel intercomparison is performed at 0.2° grid for an entire year (March 2019 to February 2020). Fig. 10 shows the spatial distribution of one-year AE (490/670) for TROPOMI/GRASP and VIIRS/DB products. The 0.2° mean difference for common pixels averaged over a year is also presented as VIIRS/DB - TROPOMI/GRASP. Here, we require the minimal occupancy of 3 over a year to calculate the differences between products. The one-year pixel-to-pixel statistics for AE (490/670) over land and ocean are summarized in Table 9.

TROPOMI/GRASP and VIIRS/DB show similar spatial distribution pattern, while the AE values are different. For example, over Southeast Asia, both two products indicate small particle dominant, while TROPOMI/GRASP (AE ~ 1.8) indicates smaller particle (larger AE) than VIIRS/DB (AE ~ 1.5). In addition, over Sahara, VIIRS/DB (AE ~ 0.2) shows coarser particle (smaller AE) than TROPOMI/GRASP (AE ~ 0.7). While, over Eastern America, VIIRS/DB shows smaller particle (AE ~ 1.5) than TROPOMI/GRASP (AE ~ 1.2). Over ocean, VIIRS/DB (AE < 0.6) shows generally coarser particle than TROPOMI/GRASP (AE ~ 1.0), which is consistent with the AERONET validation results (see in section 3.1.2) where TROPOMI/GRASP tends to overestimate slightly AE for coarse mode dominant cases. Statistically, based on >7 million pairs over land, the R between two products is ~ 0.581 with RMSE ~ 0.595 . About 56.6% and 37.8% of pairs are within Target and Optimal

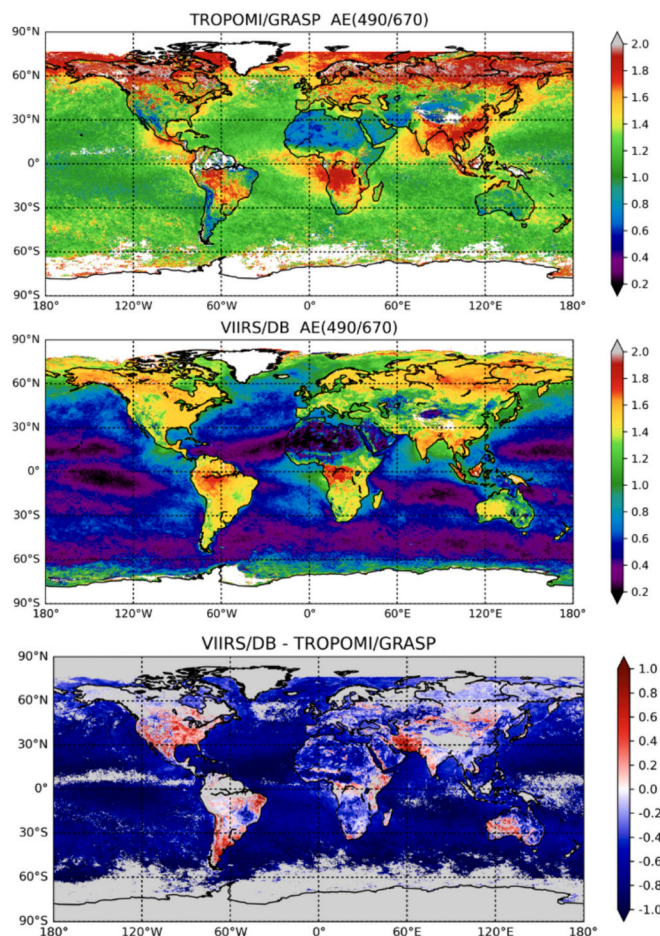


Fig. 10. Spatial distribution of one-year (March 2019 – February 2020) AE (490/670) from TROPOMI/GRASP and VIIRS/DB products. The pixel level difference of AE averaged over a year is presented as VIIRS/DB - TROPOMI/GRASP. Note only the pixels with appearances $N \geq 3$ during a year are accounted for in the difference calculation.

uncertainty requirements respectively. The mean AE difference (VIIRS/DB - TROPOMI/GRASP) is -0.254 that indicate smaller particles from TROPOMI/GRASP than VIIRS/DB. Over ocean, >13 million pairs are taken into account for intercomparison. The systematic AE difference (VIIRS/DB - TROPOMI/GRASP) (-0.712) is much more pronounced than that over land. The R is ~ 0.711 with RMSE ~ 0.808 . Because of the systematic difference, the fractions satisfying Target and Optimal uncertainty requirements, 29.4% and 15.1%, are lower than that over land.

Table 9

Summary of global pixel-to-pixel AE (490/670) statistic metrics between VIIRS/DB and TROPOMI/GRASP over land and ocean.

Land/Ocean	Products (Num. Matchups)	R	Slope	Offset	RMSE	Diff. (VIIRS - TROPOMI)	Optimal (%)	Target (%)
Land	VIIRS vs. TROPOMI (7263418)	0.581	0.823	-0.048	0.595	-0.254	37.8	56.6
Ocean	VIIRS vs. TROPOMI (13144390)	0.711	1.243	-1.033	0.808	-0.712	15.1	29.4

4.1.3. Fine and coarse mode AOD (AODF and AODC) products intercomparison

Both TROPOMI/GRASP and VIIRS/DB provide separation of fine and coarse mode AOD (AODF and AODC) over ocean. We use the same methodology as in section 3 to derive TROPOMI/GRASP and VIIRS/DB AODF and AODC at 550 nm and then re-grid them into common 0.2° grid boxes. The 0.2° pixel level inter-comparison is then performed over a year. Fig. 11 shows the spatial distribution of one-year AODF and AODC at 550 nm for TROPOMI/GRASP and VIIRS/DB products. The 0.2° pixel level difference of AODF and AODC averaged over a year is also presented as VIIRS/DB - TROPOMI/GRASP. Similar to the AOD intercomparison, we require the minimal occupancy of 10 over a year to calculate the differences between products. The pixel-to-pixel statistics for AODF and AODC over a year are summarized in Table 10.

In general, the two AODF and AODC products show similar spatial patterns over ocean, while the magnitude is different. For example, the pixel-to-pixel correlation coefficients are 0.826 for AODF and 0.916 for AODC based on >10 million pairs. Yet, VIIRS/DB AODF tends to show smaller values than TROPOMI/GRASP by about 0.034, while VIIRS/DB

AODC is higher than TROPOMI/GRASP by about 0.032. As a consequence, the VIIRS/DB total AOD (550 nm) over ocean is 0.002 smaller than TROPOMI/GRASP (Table 7). Spatially, TROPOMI/GRASP AODF is almost everywhere higher than VIIRS/DB over ocean, especially the Sahara dust across the Atlantic Ocean region, where VIIRS/DB shows much more coarse mode AOD than TROPOMI/GRASP. The Southeast Atlantic region with transported central Africa biomass burning aerosol is the only area where VIIRS/DB tends to show higher AODF than TROPOMI/GRASP. It is difficult to conclude which product is better through intercomparison. Therefore, further investigations are needed, such as the analysis of the radius of the aerosol models as well as the cutting radius to separate fine and coarse contributions.

4.1.4. SSA products intercomparison

The VIIRS/DB algorithm mainly relies on the predefined aerosol models to derive the SSA, which to some extent limits the SSA solution freedom. The VIIRS/DB SSA is diagnosed in the product and the validation with AERONET shows the deviations (RMSE) around 0.06–0.07 spectrally (Table 6-Validation). Here we compare the spatial

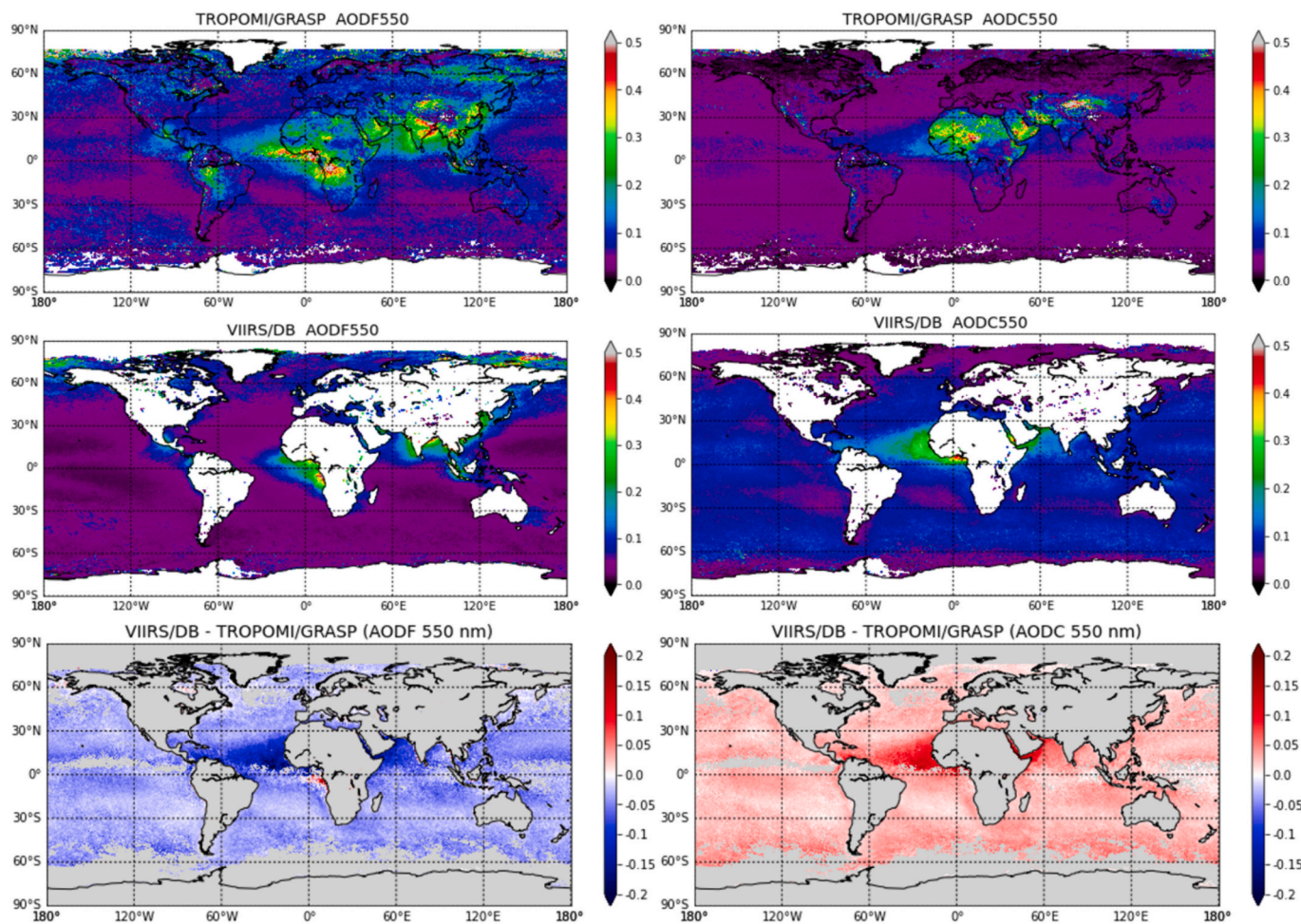


Fig. 11. Spatial distribution of one-year (March 2019 – February 2020) AODF and AODC at 550 nm from TROPOMI/GRASP and VIIRS/DB products. The pixel level difference of AODF and AODC averaged over a year is presented as VIIRS/DB - TROPOMI/GRASP. Note only the pixels with appearances $N \geq 10$ during a year are accounted for in the difference calculation.

Table 10

Summary of global pixel-to-pixel AODF and AODC at 550 nm statistic metrics between VIIRS/DB and TROPOMI/GRASP over ocean.

Land/Ocean	Products (Num. Matchups)	Bands (nm)	R	Slope	Offset	RMSE	Diff. (VIIRS - TROPOMI)	GCOS (%)	Target (%)
Ocean	AODF VIIRS vs. TROPOMI (10748159)	550	0.826	0.709	-0.009	0.060	-0.034	64.5	73.9
	AODC VIIRS vs. TROPOMI (10748159)		0.916	1.766	0.003	0.048	0.032	71.2	79.6

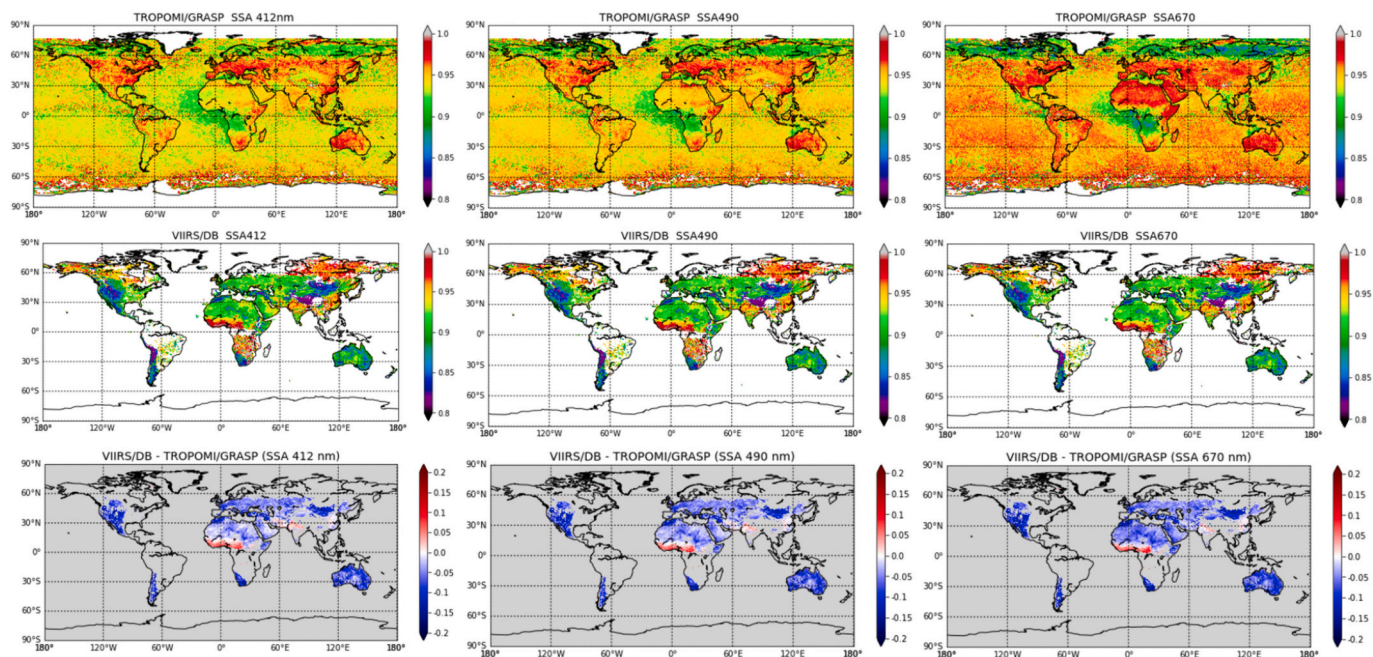


Fig. 12. Spatial distribution of one-year (March 2019 – February 2020) spectral SSA at 412, 490 and 670 nm from TROPOMI/GRASP and VIIRS/DB products. The pixel level difference of SSA averaged over a year is presented as VIIRS/DB – TROPOMI/GRASP. Note only the pixels with appearances $N \geq 10$ during a year are accounted for in the difference calculation.

Table 11

Summary of global pixel-to-pixel SSA at 412, 490 and 670 nm intercomparison statistic metrics between VIIRS/DB and TROPOMI/GRASP over land.

Land/Ocean	Products (Num. Matchups)	Bands (nm)	R	RMSE	Diff. (VIIRS - TROPOMI)	Optimal +/- 0.03 (%)	Target +/- 0.05 (%)
Land	VIIRS vs. TROPOMI (526328)	412	-0.052	0.033	0.003	75.5	86.3
		490	-0.250	0.035	-0.005	70.8	86.1
		670	-0.465	0.046	-0.023	34.8	78.2

distribution of TROPOMI/GRASP and VIIRS/DB spectral SSA at 412, 490 and 670 nm in Fig. 12, and the one-year pixel-to-pixel SSA intercomparison statistic metrics are summarized in Table 11. In general, TROPOMI/GRASP looks reasonable distributed, e.g., strong absorption (SSA is relatively low) over central and south Africa biomass burning region and the spectral dependency (the absorption capability decreases from 412 nm to 670 nm) over Sahara dust region. Over ocean, TROPOMI/GRASP SSA seems a bit underestimated by assuming the oceanic aerosol SSA 0.97–0.99 at visible channels (Dubovik et al., 2002). The underestimation is partially due to the high uncertainty of the retrieved SSA under the low aerosol loading conditions, such as over ocean. The VIIRS/DB spectral SSA show unexpected negative correlation with TROPOMI/GRASP, which may be associated with the VIIRS measurements are generally lack of sensitivity to aerosol absorption and the DB algorithm strongly relies on climatological surface database for the determination of predefined three aerosol models (mixed, dust and smoke) which limits the freedom of the SSA solutions. Despite this, there are at least 78% pixels between TROPOMI and VIIRS satisfying the SSA Target requirement (+/- 0.05). Overall, together with the validation results in section 3.1.3, TROPOMI/GRASP SSA demonstrate better accuracy than VIIRS/DB.

4.2. Surface products intercomparison

4.2.1. Intercomparison of TROPOMI and MODIS surface products

GRASP algorithm performs simultaneous retrieval of aerosol and surface BRDF properties. In order to identify the possible relations between aerosol and surface products and evaluate the global performance of the surface retrieval. TROPOMI/GRASP surface product was intercompared with MODIS MCD43 C1 (BRDF) and C3 (albedo) products (Schaaf and Wang, 2015a, 2015b). The MODIS MCD43 C1 and C3 are 0.05° gridded products, therefore we re-grid both TROPOMI and MODIS products into 0.2° spatial resolution for intercomparison. Fig. 13 shows the spatial distribution of one-year (March 2019 – February 2020) full Ross-Li BRDF (BRDF1: isotropic term; BRDF2: volumetric term; BRDF3: geometric term) (Litvinov et al., 2024) from TROPOMI/GRASP (670 nm) and MODIS MCD43C1 (Band1: 620–670 nm) products. The differences of BRDF1, BRDF2 and BRDF3 over a year are shown as MODIS - TROPOMI. Note that the annual mean is calculated from the monthly mean surface BRDF, furthermore we simply use the 15th day of each month to represent the MODIS monthly mean. Table 12 summarizes the global pixel-to-pixel full BRDF intercomparison statistic metrics between MODIS MCD43C1 and TROPOMI/GRASP at blue (440 nm) and red (670 nm) channels.

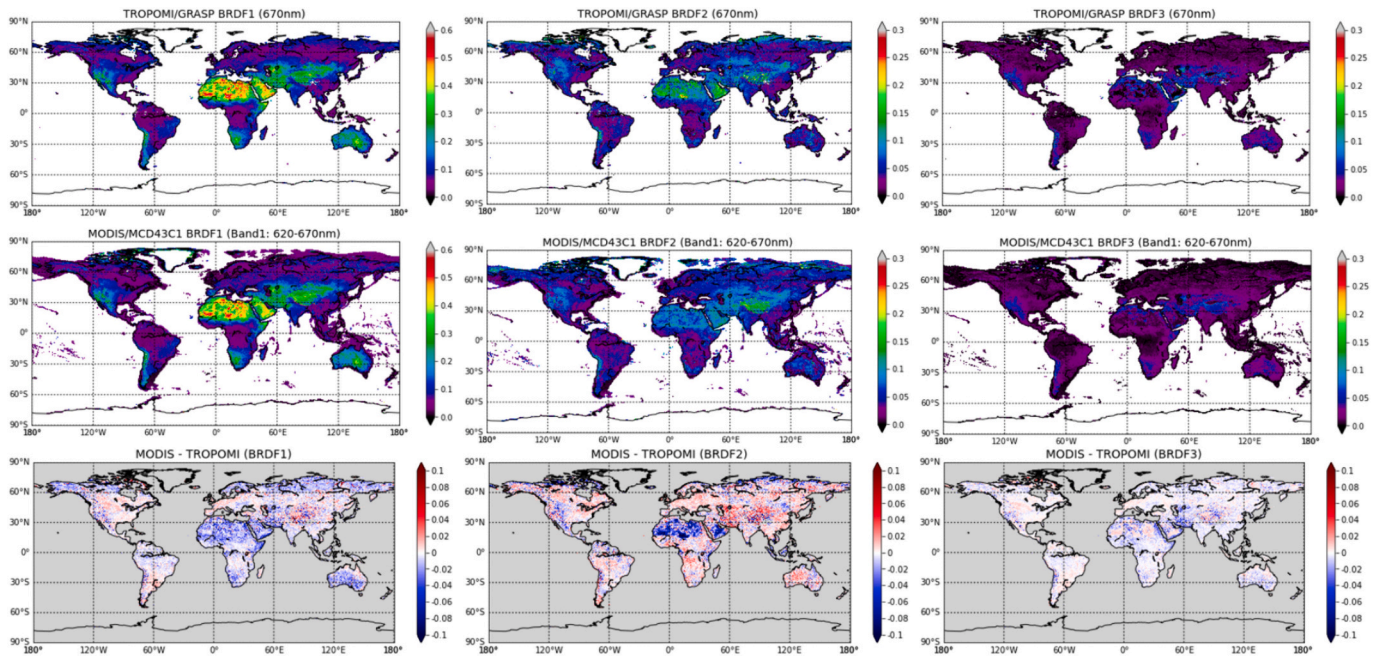


Fig. 13. Spatial distribution of one-year (March 2019 – February 2020) full BRDF (BRDF1: isotropic term; BRDF2: volumetric term; BRDF3: geometric term) from TROPOMI/GRASP (670 nm) and MODIS MCD43C1 (Band1: 620–670 nm) products at red channel. The differences of BRDF1, BRDF2 and BRDF3 over a year are shown as MODIS - TROPOMI. (For interpretation of the references to colour in this figure legend, the reader is referred to the web version of this article.)

Table 12

Summary of global pixel-to-pixel full BRDF (BRDF1: isotropic term; BRDF2: volumetric term; BRDF3: geometric term) intercomparison statistic metrics between MODIS MCD43C1 and TROPOMI/GRASP at blue and red channels.

BRDF parameters	Num. Matchups	R	RMSE	Diff. (MODIS - TROPOMI)	Optimal (%)	Target (%)
BRDF1 iso 440 nm	1,182,950	0.940	0.018	-0.004	45.1	93.2
BRDF1 iso 670 nm		0.989	0.023	-0.009	52.3	88.6
BRDF2 vol		0.652	0.033	-0.002	-	-
BRDF3 geo		0.793	0.013	-0.004	-	-

For the isotropic term (BRDF1), based on >1 million pairs, TROPOMI/GRASP show good agreement with MODIS MCD43, for example, at least 88% of pixels satisfying surface Target requirement (Litvinov et al., 2024) at blue and red channels. In addition, the correlation coefficients (R) are 0.94 at blue channel and 0.989 at red channel with RMSE around 0.018 to 0.023. The global differences (MODIS - TROPOMI) are -0.004 at blue channel and -0.009 at red channel, that MODIS is smaller than TROPOMI. Because TROPOMI/GRASP retrieves spectral independent volumetric and geometric terms (see details in Part I of Litvinov et al. (2024)), we therefore compare MODIS/MCD43 Band 1 BRDF2 and BRDF3 with TROPOMI/GRASP. Even though the global difference (MODIS - TROPOMI) is smallest (-0.002) for BRDF2, the deviation (RMSE) is the highest (0.033). Over the Sahara Desert, TROPOMI/GRASP tends to have higher BRDF2 than MODIS, while it tends to be randomly distributed over other regions. For the geometric term (BRDF3), the agreement between TROPOMI and MODIS is generally good with global difference 0.004 and RMSE 0.013. There are no evident regional biases between the two products.

From the directly retrieved full BRDF parameters, both TROPOMI and MODIS derive surface albedos, such as white sky albedo and black sky albedo. Here we compare one-year TROPOMI/GRASP and MODIS MCD43C3 white sky albedo at blue and red channels in Fig. 14. Table 13 summarizes the global pixel-to-pixel white sky albedo intercomparison statistic metrics between MODIS and TROPOMI. In general, two products show similar spatial distribution, although some minor discrepancies can be observed, e.g., TROPOMI is lower than MODIS at 440 nm, while it is higher than MODIS at 670 nm over the Sahara. According to

the pixel-to-pixel statistics, the dispersions between 2 products are within 0.02 at 440 and 670 nm (RMSE 0.016–0.017), the global differences are nearly zeros (-0.002 - -0.007), and ~96% pixels fall in the Target requirement and >~45% pixels satisfy the Optimal requirement. Taking into account the differences of center wavelengths from 2 different instruments, and MODIS products are accumulated of 16-days TERRA and AQUA data and weighted to the day of interest, the overall global difference is reasonable.

4.2.2. Intercomparison of TROPOMI and SCIAMACHY, OMI, GOME-2 surface LER climatology

The summary of TROPOMI/GRASP pixel-to-pixel statistic metrics with the OMI, GOME-2 and SCIAMACHY surface LER climatology are listed in Tables 14–16. Due to the 0.25–0.5° spatial resolution of the climatological datasets, we re-grid all of them into 0.5° grid box and then conduct the intercomparison. Generally, the results are consistent with the evaluation of surface products with GROSAT surface reference dataset over AERONET sites in Section 3.2. TROPOMI/GRASP shows good correspondence between OMI in the spectrum range (340–490 nm) with RMSE ~0.02 and the difference (OMI - TROPOMI) within +/- 0.01, especially in the UV (367–380 nm) range that the differences is nearly zeros. The intercomparisons between TROPOMI with GOME-2 (Table 15) and SCIAMACHY (Table 16) also show good correspondence in the spectrum range 380 to 490 nm, where the dispersion RMSE is generally lower than 0.025. The TROPOMI/GRASP tends to be a bit higher than OMI, GOME-2 and SCIAMACHY at 340 nm around 0.01–0.018, and the difference decreases to nearly zero at 490 nm.

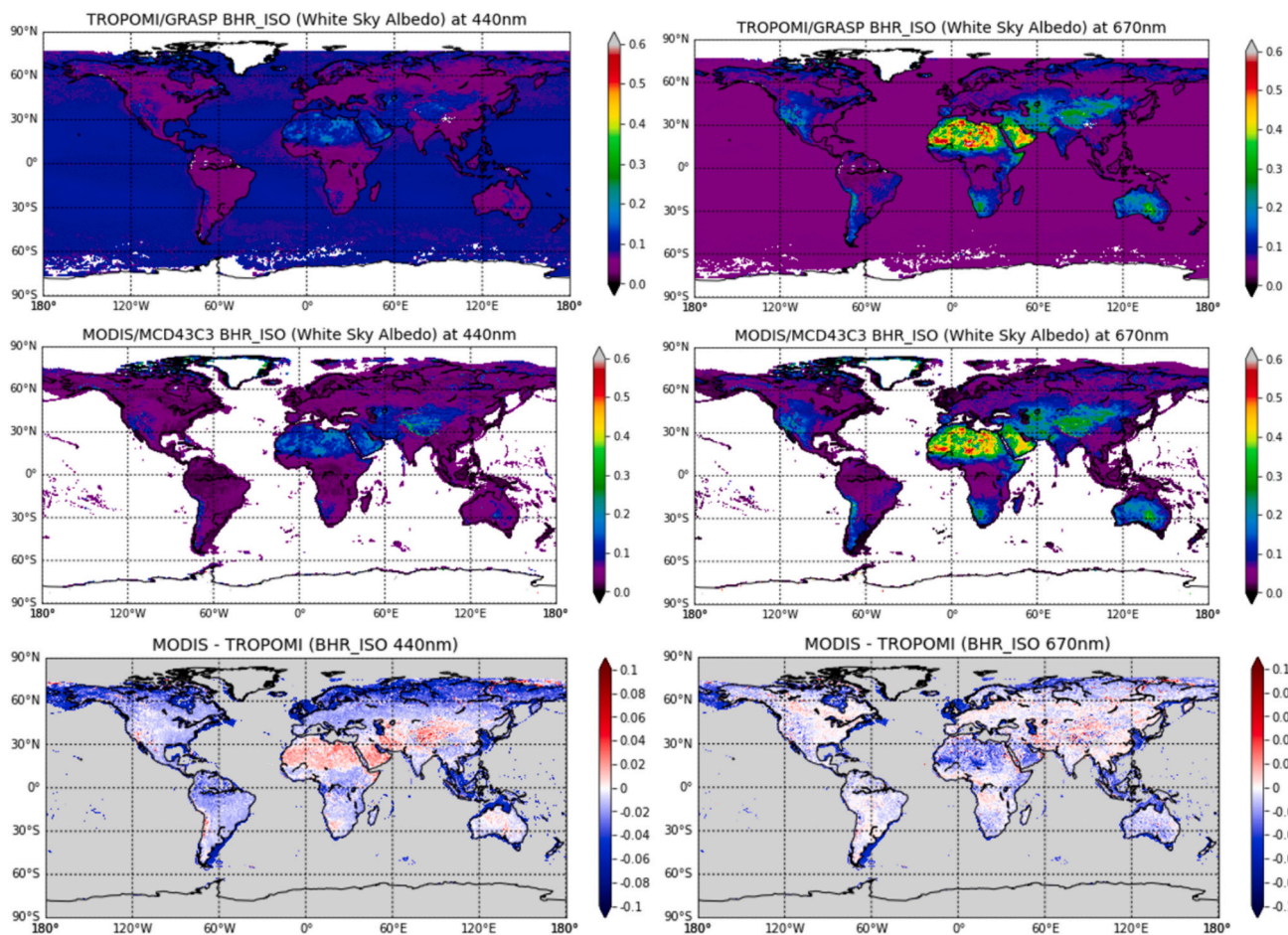


Fig. 14. Spatial distribution of one-year (March 2019 – February 2020) white sky albedo (BHR_ISO) from TROPOMI/GRASP and MODIS MCD43C3 products at blue and red channels. The BHR_ISO differences over a year are shown as MODIS - TROPOMI. (For interpretation of the references to colour in this figure legend, the reader is referred to the web version of this article.)

Table 13

Summary of global pixel-to-pixel BHR_ISO (white sky albedo) intercomparison statistic metrics between MODIS MCD43C3 and TROPOMI/GRASP at blue and red channels.

Wavelengths (nm)	Num. Matchups	R	RMSE	Diff. (MODIS - TROPOMI)	Optimal (%)	Target (%)
440	1,200,760	0.955	0.016	-0.002	45.1	95.6
670		0.994	0.017	-0.007	63.3	95.9

Table 14

Summary of global pixel-to-pixel intercomparison statistic metrics between OMI LER climatology and TROPOMI/GRASP BHR_ISO at all common wavelengths from UV to green.

Wavelengths (nm)	Num. Matchups	R	RMSE	Diff. (OMI - TROPOMI)	Optimal (%)	Target (%)
340	191,695	0.432	0.023	-0.011	30.9	58.4
367		0.604	0.021	-0.006	34.2	63.5
380		0.703	0.020	0.000	34.8	66.2
416		0.871	0.021	0.010	33.5	66.4
440		0.916	0.021	0.010	34.6	67.9
494		0.947	0.021	0.010	35.9	67.4

While, in the spectrum range red (670 nm) to NIR and SWIR, TROPOMI/GRASP tends to provide higher albedo (~0.03–0.04) than the climatological datasets (GOME-2 and SCIAMACHY). According to the validation with the surface reference dataset, all 3 products (TROPOMI/GRASP, GOME-2 and SCIAMACHY) tend to underestimate from Red to NIR and SWIR channels, where the underestimation for TROPOMI/GRASP (0.01–0.015) is not as strong as for GOME-2 (~0.03–0.04) and

SCIAMACHY (0.03–0.05). This may explain the differences seen for TROPOMI/GRASP, GOME-2 and SCIAMACHY global pixel-to-pixel inter-comparisons from red to NIR and SWIR channels.

Fig. 15 shows the spatial distribution of August 2019 monthly TROPOMI/GRASP White Sky Albedo (BHR_ISO) and its difference with SCIAMACHY, GOME-2 and OMI LER albedo climatology for August at 380, 494, 772 and 2313 nm. Even though, the global differences

Table 15

Summary of global pixel-to-pixel intercomparison statistic metrics between GOME-2 LER climatology and TROPOMI/GRASP BHR_ISO at all common wavelengths from UV to NIR.

Wavelengths (nm)	Num. Matchups	R	RMSE	Diff. (GOME-2 – TROPOMI)	Optimal (%)	Target (%)
340	191,514	0.259	0.028	−0.009	24.7	48.9
367		0.511	0.026	−0.003	26.2	53.7
380		0.639	0.025	0.005	31.9	61.0
416		0.842	0.023	0.005	37.0	67.5
440		0.893	0.022	0.003	38.7	68.8
494		0.924	0.024	0.000	37.3	65.9
670		0.955	0.050	−0.026	19.6	39.4
747		0.931	0.053	−0.030	14.5	29.8
772		0.925	0.058	−0.036	11.9	24.7

Table 16

Summary of global pixel-to-pixel intercomparison statistic metrics between SCIAMACHY LER climatology and TROPOMI/GRASP BHR_ISO at all common wavelengths from UV to SWIR.

Wavelengths (nm)	Num. Matchups	R	RMSE	Diff. (SCIAMACHY – TROPOMI)	Optimal (%)	Target (%)
340	191,839	0.393	0.030	−0.018	23.4	44.4
367		0.593	0.027	−0.013	25.6	49.2
380		0.692	0.023	−0.007	27.0	55.1
416		0.860	0.022	0.002	31.0	65.3
440		0.902	0.020	−0.002	36.3	71.4
494		0.934	0.021	−0.004	39.5	71.3
670		0.962	0.046	−0.028	18.8	39.0
747		0.931	0.054	−0.034	13.2	26.8
772		0.924	0.063	−0.045	9.0	18.8
2313		0.952	0.058	−0.022	17.4	34.6

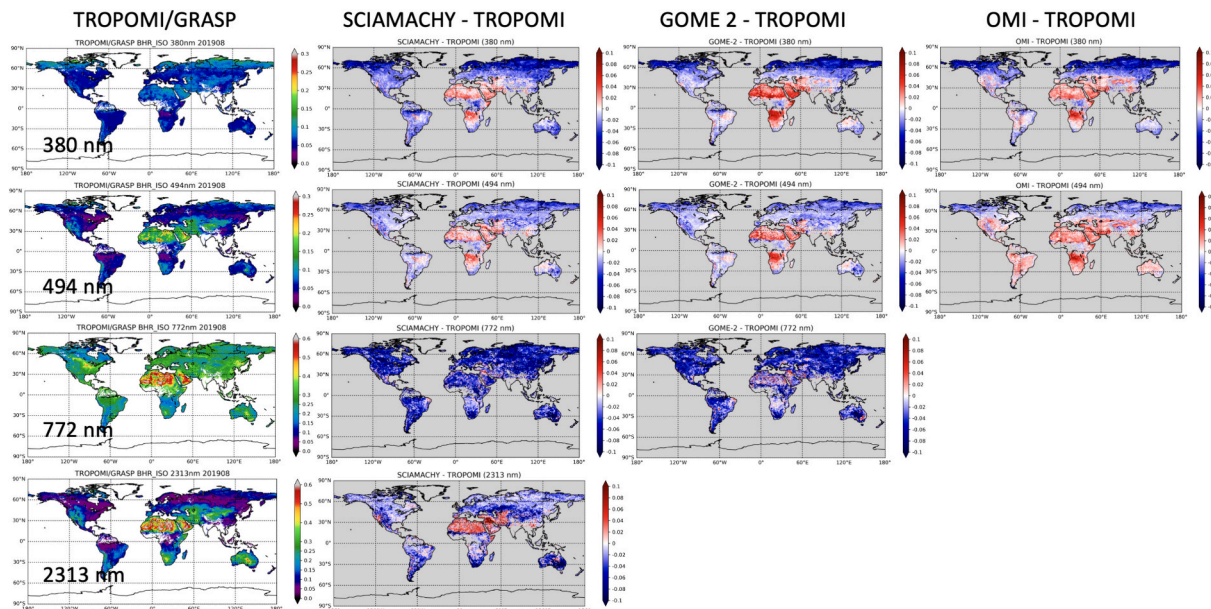


Fig. 15. Spatial distribution of monthly (August 2019) surface albedo from TROPOMI/GRASP (BHR_ISO) and its difference with SCIAMACHY, GOME-2 and OMI LER albedo climatology for August at 380, 494, 772 and 2313 nm.

between TROPOMI and SCIAMACHY, GOME-2 and OMI climatology do not exceed ± 0.01 at 380 nm, spatially the tendency is evident and consistent with 3 KNMI climatological datasets (OMI, GOME-2 and SCIAMACHY) (Kleipool et al., 2008; Tilstra et al., 2021; Tilstra et al., 2017) that TROPOMI shows higher surface albedo over northern hemisphere high latitudes and lower surface albedo over deserts and southern hemisphere Africa area with strong biomass burning emissions in June – September. At 494 nm, the spatial pattern is similar to 380 nm and the absolute differences are smaller than that of 380 nm. As shown in pixel-to-pixel intercomparison in Tables 14–16, the largest difference

is observed at 772 nm, where GOME-2 and SCIAMACHY LER is generally lower than TROPOMI/GRASP with the global mean difference ~ 0.03 – 0.045 . At SWIR 2313 nm, SCIAMACHY tends to report higher albedo over deserts and lower albedo over other areas. On one hand, these differences can be explained to some extent by different sampling: SCIAMACHY, GOME-2 and OMI climatology are based on the data accumulated over different time periods with TROPOMI, and, in addition, the datasets are generated under different spatial resolution. On the other hand, the difference is unexpected at the SWIR channel where the surface contribution is dominant. One of the potential reasons is the

utilization of the spectral smoothness of GRASP approach, while it is in generally mild constraint with Lagrange multiplier $1.0e-8$. Therefore, further investigations are needed here.

5. Summary and conclusion

This study firstly presents the systematic intercomparison of S5P-TROPOMI/GRASP aerosol and surface products globally with 2 aerosol datasets (MODIS/TERR DT + DB and VIIRS/DB) and 2 surface datasets (MODIS/MCD43 BRDF and albedo and surface LER climatology from SCIAMACHY, OMI and GOME-2). As part of the intercomparison exercise, we validated these aerosol and surface datasets using the same validation methodology with AERONET aerosol reference dataset and the surface reference dataset generated from S5P-TROPOMI and AERONET synergistic retrieval and the validation metrics are intercompared.

5.1. Aerosol retrieval intercomparison

TROPOMI and VIIRS are 2 independent instruments flying within ~3–5 minutes, and the aerosol products are generated based on 2 independent algorithms (TROPOMI/GRASP and VIIRS/DB). As a main result, we should mention a remarkable agreement between two aerosol products, specifically for the spectral AOD, from deep blue channel (412 nm) to the red channel (670 nm) over ocean and different land surfaces. Generally, over ocean >85% matchup AOD (550 nm) pairs are within GCOS uncertainties and pixel-to-pixel Pearson correlation coefficient (R) is higher than 0.95 with average absolute difference within ± 0.002 . Over land the pixel-to-pixel R are higher than 0.85 and differences are within ± 0.016 for four classes of NDVIs ($0 < NDVI \leq 0.2$, $0.2 < NDVI \leq 0.4$, $0.4 < NDVI \leq 0.6$, and $0.6 < NDVI \leq 1$). >46% of pairs are within GCOS uncertainties.

The TROPOMI/GRASP and MODIS/TERRA DT + DB AOD (550 nm) are also intercompared, and the agreement is generally a bit less good than that between TROPOMI/GRASP and VIIRS/DB. There are evident differences that MODIS/TERR DT + DB AOD (550 nm) is lower (-0.092) over bright surface ($0 < NDVI \leq 0.2$) and is higher ($+0.037$) over dense vegetation surface ($0.6 < NDVI \leq 1$) than TROPOMI/GRASP. Over areas with NDVI between 0.2 and 0.6, the agreement between MODIS and TROPOMI is much better with difference within ± 0.02 , although it is still larger than that between VIIRS/DB and TROPOMI/GRASP.

The AE (490/670) intercomparison is also performed between TROPOMI/GRASP and VIIRS/DB. Although the Pearson correlation coefficient (R) between two products is reasonable at ~ 0.7 , the systematic difference (~ 0.712) is observed and pronounced over ocean where TROPOMI/GRASP shows larger AE (smaller particle) than VIIRS/DB. As a result, the fractions within the Optimal and Target uncertainty requirements are a bit smaller (15.1% and 29.4%) over ocean than that (37.8% and 56.6%) over land. The R is smaller over land (~ 0.581) than that over ocean. Some discrepancies are observed over land. For example, VIIRS/DB shows smaller AE (~ 0.2) than TROPOMI/GRASP (~ 0.9) over Sahara Desert, and VIIRS/DB shows larger AE (~ 1.5) than TROPOMI/GRASP (~ 1.2) over Eastern America.

As for AODF and AODC at 550 nm over ocean, both products (TROPOMI/GRASP and VIIRS/DB) show reasonable agreement with AERONET coastal sites validation, while TROPOMI/GRASP tends to underestimate high AODC cases and VIIRS/DB seems to overestimate AODC. As a consequence, although the global pixel-to-pixel AODF and AODC correlations are higher than 0.82 and >64% pairs satisfying GCOS requirements, the clear differences are observed that VIIRS/DB reports lower (-0.034) AODF and higher ($+0.032$) AODC than TROPOMI/GRASP.

Even though VIIRS/DB diagnosed SSA over land are of 0.06–0.07 deviation (RMSE) with AERONET inversion products, TROPOMI/GRASP show much better agreement with AERONET with RMSE ~ 0.026 at 490 nm and 82.6% pairs are within SSA Optimal requirement (\pm

0.03). Globally, the pixel-to-pixel correlation between the two products is poor, while the differences are generally within ± 0.05 for most of the cases (>80%). Overall, based on the validation with AERONET, TROPOMI/GRASP SSA are of better confidence and accuracy than SSA from VIIRS/DB. As it was discussed in Part I (Litvinov et al., 2024) the better performance in SSA can be the result of combining advanced possibilities of GRASP algorithm and extended information content provided by S5P/TROPOMI from UV to SWIR spectral measurements, specifically S5P/TROPOMI wide spectral range, wide swath and frequent overpass combined with the GRASP multi-pixel approach.

5.2. Surface retrieval intercomparison

The intercomparison of TROPOMI/GRASP and MODIS/MCD43 surface products show very good mutual correspondence for common channels 440 nm (blue) and 670 nm (red) for both the full set of Ross-Li BRDF parameters and white sky albedo. The global pixel-to-pixel MODIS and TROPOMI white sky albedo show $R \sim 0.955$ at 440 nm and ~ 0.994 at 670 nm, and the RMSEs are 0.016–0.017 with at least 95% pairs satisfying surface Target requirements. The global pixel-to-pixel absolute mean differences are around 0.002–0.007 that MODIS is lower than TROPOMI. By considering the products are derived from two different instruments from different algorithms, the observed global differences are reasonable.

The inter-comparison of TROPOMI/GRASP white sky albedo with OMI, GOME-2 and SCIAMACHY climatological LER demonstrates reasonable correspondence taken into account different spatial distribution and different definition of the surface products (White Sky Albedo – BHR_ISO from TROPOMI/GRASP vs. LER from other instruments). In general, the intercomparison reveals that the correspondence of the datasets is much better for the visible channels (416–490 nm) than Red-NIR-SWIR (670–2313 nm) channels. In the spectrum range 416–490 nm, both products agree to each other well with the absolute difference between ± 0.01 . In the spectrum Red-NIR-SWIR, GOME-2 and SCIAMACHY climatology tends to report smaller LER values (0.02–0.045) than TROPOMI/GRASP BHR_ISO. According to the validation with surface reference dataset, all the datasets are underestimated at this spectrum range, where the underestimation for TROPOMI/GRASP (0.01–0.02) is smaller than for GOME-2 (~ 0.03) and SCIAMACHY (0.03–0.05). In UV spectrum 340–380 nm, a reasonable pixel-to-pixel agreement is observed, e.g., the differences between OMI, GOME-2 and TROPOMI are within 0.02, and TROPOMI/GRASP is always higher than OMI and GOME-2.

Overall, the validation and intercomparison of S5P-TROPOMI/GRASP aerosol and surface products, performed using the ground-based, satellite measurements as well as the aerosol surface reference datasets, show high percentage of the TROPOMI/GRASP aerosol and surface retrieved characteristics, which meet the formulated requirements. Provided detailed aerosol/surface information, including spectral AOD, fine/coarse mode AOD, AAOD, SSA, full BRDF characterization etc. at UV, VIS, NIR and SWIR spectrum, is crucial for different environmental studies in general and specifically for aerosol climate effects evaluation.

CRedit authorship contribution statement

Cheng Chen: Writing – review & editing, Writing – original draft, Visualization, Validation, Methodology, Formal analysis, Conceptualization. **Pavel Litvinov:** Writing – review & editing, Writing – original draft, Resources, Methodology, Investigation, Conceptualization. **Oleg Dubovik:** Writing – review & editing, Resources, Investigation, Conceptualization. **Lukas Bindreiter:** Software, Data curation. **Christian Matar:** Writing – review & editing, Project administration, Funding acquisition. **David Fuentes:** Software, Resources, Data curation. **Anton Lopatin:** Writing – review & editing, Investigation. **Tatyana Lapyonok:** Investigation. **Verena Lanzinger:** Software, Data curation. **Andreas**

Hangler: Software, Data curation. **Michael Aspetsberger:** Software, Resources, Data curation. **Martin de Graaf:** Writing – review & editing, Investigation. **Lieuwe Gijbert Tilstra:** Writing – review & editing, Investigation. **Piet Stammes:** Writing – review & editing, Investigation. **Alexandru Dandocsi:** Writing – review & editing. **Daniele Gasbarra:** Writing – review & editing. **Elody Fluck:** Investigation. **Claus Zehner:** Writing – review & editing, Funding acquisition. **Christian Retscher:** Writing – review & editing, Project administration, Funding acquisition.

Declaration of competing interest

The authors declare that they have no known competing financial interests or personal relationships that could have appeared to influence the work reported in this paper.

Appendix A

Table A1

Statistical metrics of validation of TROPOMI/GRASP white sky albedo (or BHR_ISO) with GROSAT S5P/TROPOMI surface reference dataset.

TROPOMI/GRASP vs. TROPOMI/GROSAT	Wavelengths (nm)	RMSE	BIAS	Optimal (%)	Target (%)
	340	0.027	-0.009	31.8	58.8
	367	0.024	-0.010	36.7	65.1
	380	0.022	-0.008	38.8	68.1
	416	0.019	-0.006	43.8	73.5
	440	0.018	-0.006	46.0	76.2
	494	0.015	-0.005	51.7	81.9
	670	0.019	-0.006	49.1	75.7
	747	0.031	-0.012	29.8	53.5
	772	0.035	-0.013	27.6	50.1
	2313	0.022	-0.009	42.5	69.4
	All	0.024	-0.008	39.8	67.2

Table A2

Statistical metrics of validation of MODIS/MCD43C3 white sky albedo (or BHR_ISO) with GROSAT S5P/TROPOMI surface reference dataset.

MODIS/MCD43C3 vs. TROPOMI/GROSAT	Wavelengths (nm)	RMSE	BIAS	Optimal (%)	Target (%)
	465 vs. 440	0.016	-0.012	38.8	81.4
	645 vs. 670	0.020	-0.010	43.0	70.5
	All	0.018	-0.011	40.9	75.9

Table A3

Statistical metrics of validation of SCIAMACHY climatological LER with GROSAT S5P/TROPOMI surface reference dataset (BHR_ISO).

SCIAMACHY vs. TROPOMI/GROSAT	Wavelengths (nm)	RMSE	BIAS	Optimal (%)	Target (%)
	340	0.039	-0.033	7.7	25.3
	367	0.033	-0.026	11.9	31.4
	380	0.026	-0.018	19.1	44.8
	416	0.022	-0.011	26.8	61.3
	440	0.022	-0.011	31.4	62.4
	494	0.022	-0.011	27.3	61.9
	670	0.040	-0.030	10.3	29.9
	747	0.058	-0.037	9.8	24.2
	772	0.069	-0.051	8.2	16.5
	2313	0.047	-0.033	13.4	24.2
	All	0.041	-0.026	16.6	16.6

Table A4

Statistical metrics of validation of OMI climatological LER with GROSAT S5P/TROPOMI surface reference dataset (BHR_ISO).

OMI vs. TROPOMI/GROSAT	Wavelengths (nm)	RMSE	BIAS	Optimal (%)	Target (%)
	340	0.035	-0.027	10.6	26.6
	367	0.030	-0.020	17.9	42.7
	380	0.025	-0.012	26.1	57.3
	416	0.022	0.001	40.8	68.8
	440	0.022	0.003	44.0	68.8
	494	0.024	0.005	39.9	65.1
	All	0.027	-0.008	29.9	54.9

Table A5

Statistical metrics of validation of GOME-2 climatological LER with GROSAT S5P/TROPOMI surface reference dataset (BHR_ISO).

GOME-2 vs. TROPOMI/GROSAT	Wavelengths (nm)	RMSE	BIAS	Optimal (%)	Target (%)
	340	0.036	-0.028	10.0	25.9
	367	0.029	-0.020	14.9	40.3
	380	0.023	-0.010	27.9	59.7
	416	0.021	-0.006	35.3	67.2
	440	0.022	-0.006	34.3	69.7
	494	0.024	-0.007	28.9	62.7
	670	0.041	-0.028	14.4	30.3
	747	0.056	-0.034	13.9	26.4
	772	0.065	-0.045	12.4	20.9
	All	0.038	-0.020	21.3	44.8

References

- Bréon, F.-M., Vermeulen, A., Desclotres, J., 2011. An evaluation of satellite aerosol products against sunphotometer measurements. *Remote Sens. Environ.* 115 (12), 3102–3111. <https://doi.org/10.1016/j.rse.2011.06.017>.
- Cao, C., Xiong, J., Blonski, S., Liu, Q., Uprety, S., Shao, X., et al., 2013. Suomi NPP VIIRS sensor data record verification, validation, and long-term performance monitoring. *J. Geophys. Res. Atmos.* 118 (20), 11, 664–11,678. <https://doi.org/10.1002/2013JD020418>.
- Cao, C., Blonski, S., Wang, W., Uprety, S., Shao, X., Choi, J., Lynch, E., Kalluri, S., 2018. NOAA-20 VIIRS on-orbit performance, data quality, and operational Cal/Val support. *Proc. SPIE* 10781, 63–71. <https://doi.org/10.1117/12.2324329>.
- Chen, C., Dubovik, O., Fuertes, D., Litvinov, P., Lapyonok, T., Lopatin, A., et al., 2020. Validation of GRASP algorithm product from POLDER/PARASOL data and assessment of multi-angular polarimetry potential for aerosol monitoring. *Earth System Science Data* 12 (4), 3573–3620. <https://doi.org/10.5194/essd-12-3573-2020>.
- Chen, C., Dubovik, O., Schuster, G.L., Chin, M., Henze, D.K., Lapyonok, T., et al., 2022a. Multi-angular polarimetric remote sensing to pinpoint global aerosol absorption and direct radiative forcing. *Nat. Commun.* 13 (1), 1–11. <https://doi.org/10.1038/s41467-022-35147-y>.
- Chen, C., Dubovik, O., Litvinov, P., Fuertes, D., Lopatin, A., Lapyonok, T., et al., 2022b. Properties of aerosol and surface derived from OLCI / Sentinel-3A using GRASP approach: Retrieval development and preliminary validation. *Remote Sens. Environ.* 280 (June), 113142. <https://doi.org/10.1016/j.rse.2022.113142>.
- Cox, C., Munk, W., 1954. Measurement of the roughness of the sea surface from photographs of the Sun's glitter. *J. Opt. Soc. Am.* 44 (11), 838. <https://doi.org/10.1364/josa.44.000838>.
- de Leeuw, G., Holzer-Popp, T., Bevan, S., Davies, W.H., Desclotres, J., Grainger, R.G., et al., 2015. Evaluation of seven European aerosol optical depth retrieval algorithms for climate analysis. *Remote Sens. Environ.* 162, 295–315. <https://doi.org/10.1016/j.rse.2013.04.023>.
- Diner, D.J., Beckert, J.C., Reilly, T.H., Bruegge, C.J., Conel, J.E., Kahn, R.A., et al., 1998. Multi-angle imaging Spectroradiometer (MISR) instrument description and experiment overview. *IEEE Trans. Geosci. Remote Sens.* 36 (4), 1072–1087. <https://doi.org/10.1109/36.700992>.
- Dubovik, O., King, M.D., 2000. A flexible inversion algorithm for retrieval of aerosol optical properties from sun and sky radiance measurements. *J. Geophys. Res. Atmos.* 105 (D16), 20673–20696. <https://doi.org/10.1029/2000JD900282>.
- Dubovik, O., Smirnov, A., Holben, B.N., King, M.D., Kaufman, Y.J., Eck, T.F., Slutsker, I., 2000. Accuracy assessments of aerosol optical properties retrieved from aerosol robotic network (AERONET) sun and sky radiance measurements. *J. Geophys. Res. Atmos.* 105 (D8), 9791–9806. <https://doi.org/10.1029/2000JD900040>.
- Dubovik, O., Holben, B., Eck, T.F., Smirnov, A., Kaufman, Y.J., King, M.D., et al., 2002. Variability of absorption and optical properties of key aerosol types observed in worldwide locations. *J. Atmos. Sci.* 59 (3), 590–608. [https://doi.org/10.1175/1520-0469\(2002\)059<0590:VOAAOP>2.0.CO;2](https://doi.org/10.1175/1520-0469(2002)059<0590:VOAAOP>2.0.CO;2).
- Dubovik, O., Sinyuk, A., Lapyonok, T., Holben, B.N., Mishchenko, M., Yang, P., et al., 2006. Application of spheroid models to account for aerosol particle nonsphericity in remote sensing of desert dust. *J. Geophys. Res.* 111 (D11), D11208. <https://doi.org/10.1029/2005JD006619>.
- Dubovik, O., Herman, M., Holdak, A., Lapyonok, T., Tanré, D., Deuzé, J.L., et al., 2011. Statistically optimized inversion algorithm for enhanced retrieval of aerosol properties from spectral multi-angle polarimetric satellite observations. *Atmos. Meas. Tech.* 4 (5), 975–1018. <https://doi.org/10.5194/amt-4-975-2011>.
- Dubovik, O., Lapyonok, T., Litvinov, P., Herman, M., Fuertes, D., Ducos, F., et al., 2014. GRASP: a versatile algorithm for characterizing the atmosphere. *SPIE Newsroom*. <https://doi.org/10.1117/2.1201408.005558>.
- Dubovik, O., Fuertes, D., Lytvynov, P., Lopatin, A., Lapyonok, T., Dubovik, I., et al., 2021a. A comprehensive description of multi-term LSM for applying multiple a priori constraints in problems of atmospheric remote sensing: GRASP algorithm, concept, and applications. *Front. Remote Sensing* 1–23. <https://doi.org/10.3389/FRSEN.2021.706851>.
- Dubovik, O., Schuster, G.L., Xu, F., Hu, Y., Bösch, H., Landgraf, J., Li, Z., 2021b. Grand challenges in satellite remote sensing. *Front. Remote Sensing* 2 (February), 619818. <https://doi.org/10.3389/frsen.2020.603650>.
- Eck, T.F., Holben, B.N., Reid, J.S., Dubovik, O., Smirnov, A., O'Neill, N.T., et al., 1999. Wavelength dependence of the optical depth of biomass burning, urban, and desert dust aerosols. *J. Geophys. Res. Atmos.* 104 (D24), 31333–31349. <https://doi.org/10.1029/1999JD900923>.
- Forster, P., Alterskjær, K., Smith, C., Colman, R., Damon Matthews, H., Ramaswamy, V., et al., 2021. The Earth's energy budget, climate feedbacks and climate sensitivity. In: Masson-Delmotte, V., Zhai, P., Pirani, A., Connors, S., Péan, C., Berger, S., et al. (Eds.), *Climate Change 2021: The Physical Science Basis. Contribution of Working Group I to the Sixth Assessment Report of the Intergovernmental Panel on Climate Change*. Cambridge University Press, Cambridge, United Kingdom and New York, NY, USA, pp. 923–1054. <https://doi.org/10.1017/9781009157896.009>.
- Frouin, R., Pelletier, B., 2015. Bayesian methodology for inverting satellite ocean-color data. *Remote Sens. Environ.* 159, 332–360. <https://doi.org/10.1016/j.rse.2014.12.001>.
- Frouin, R., Schwindling, M., Deschamps, P.Y., 1996. Spectral reflectance of sea foam in the visible and near-infrared: in situ measurements and remote sensing implications. *J. Geophys. Res. C Oceans* 101 (C6), 14361–14371. <https://doi.org/10.1029/96JC00629>.
- Giles, D.M., Sinyuk, A., Sorokin, M.G., Schafer, J.S., Smirnov, A., Slutsker, I., et al., 2019. Advancements in the aerosol robotic network (AERONET) version 3 database – automated near-real-time quality control algorithm with improved cloud screening for sun photometer aerosol optical depth (AOD) measurements. *Atmos. Meas. Tech.* 12 (1), 169–209. <https://doi.org/10.5194/amt-12-169-2019>.
- Holben, B.N., Eck, T.F., Slutsker, I., Tanré, D., Buis, J.P., Setzer, A., et al., 1998. AERONET—A federated instrument network and data archive for aerosol characterization. *Remote Sens. Environ.* 66 (1), 1–16. [https://doi.org/10.1016/S0034-4257\(98\)00031-5](https://doi.org/10.1016/S0034-4257(98)00031-5).
- Holzer-Popp, T., de Leeuw, G., Griesfeller, J., Martynenko, D., Klüser, L., Bevan, S., et al., 2013. Aerosol retrieval experiments in the ESA Aerosol cci project. *Atmos. Meas. Tech.* 6 (8), 1919–1957. <https://doi.org/10.5194/amt-6-1919-2013>.
- Hsu, N.C., Tsay, S.-C., King, M.D., Herman, J.R., 2004. Aerosol properties over bright-reflecting source regions. *IEEE Trans. Geosci. Remote Sens.* 42 (3), 557–569. <https://doi.org/10.1109/TGRS.2004.824067>.

- Hsu, N.C., Tsay, S.-C., King, M.D., Herman, J.R., 2006. Deep blue retrievals of Asian aerosol properties during ACE-Asia. *IEEE Trans. Geosci. Remote Sens.* 44 (11), 3180–3195. <https://doi.org/10.1109/TGRS.2006.879540>.
- Hsu, N.C., Jeong, M.-J., Bettenhausen, C., Sayer, A.M., Hansell, R., Seftor, C.S., et al., 2013. Enhanced deep blue aerosol retrieval algorithm: the second generation. *J. Geophys. Res. Atmos.* 118 (16), 9296–9315. <https://doi.org/10.1002/jgrd.50712>.
- Hsu, N.C., Lee, J., Sayer, A.M., Kim, W., Bettenhausen, C., Tsay, S.-C., 2019. VIIRS deep blue aerosol products over land: extending the EOS long-term aerosol data records. *J. Geophys. Res. Atmos.* 124 (7), 4026–4053. <https://doi.org/10.1029/2018JD029688>.
- Hubanks, P.A., 2017. MODIS Atmosphere QA Plan for Collection 061. Greenbelt, MD USA.
- Kaufman, Y.J., Tanré, D., Remer, L.A., Vermote, E.F., Chu, A., Holben, B.N., 1997. Operational remote sensing of tropospheric aerosol over land from EOS moderate resolution imaging spectroradiometer. *J. Geophys. Res. Atmos.* 102 (D14), 17051–17067. <https://doi.org/10.1029/96jd03988>.
- Kaufman, Yoram J., Tanré, D., Boucher, O., 2002. A satellite view of aerosols in the climate system. *Nature* 419 (6903), 215–223. <https://doi.org/10.1038/nature01091>.
- King, M.D., 1999. EOS Science Plan: The State of Science in the EOS Program. NASA, Washington, D. C.
- King, M.D., Kaufman, Y.J., Tanré, D., Nakajima, T., 1999. Remote sensing of tropospheric aerosols from space: past, present, and future. *Bull. Am. Meteorol. Soc.* 80 (11), 2229–2259. [https://doi.org/10.1175/1520-0477\(1999\)080<2229:RSOTAF>2.0.CO;2](https://doi.org/10.1175/1520-0477(1999)080<2229:RSOTAF>2.0.CO;2).
- Kleipool, Q.L., Dobber, M.R., de Haan, J.F., Levelt, P.F., 2008. Earth surface reflectance climatology from 3 years of OMI data. *J. Geophys. Res. Atmos.* 113 (18), 1–22. <https://doi.org/10.1029/2008JD010290>.
- Koepke, P., 1984. Effective reflectance of oceanic whitecaps. *Appl. Opt.* 23 (11), 1816–1824. <https://doi.org/10.1364/AO.23.001816>.
- Kokhanovsky, A.A., Breon, F.M., Cacciari, A., Carboni, E., Diner, D., di Nicolantonio, W., et al., 2007. Aerosol remote sensing over land: A comparison of satellite retrievals using different algorithms and instruments. *Atmos. Res.* 85 (3–4), 372–394. <https://doi.org/10.1016/j.atmosres.2007.02.008>.
- Kokhanovsky, A.A., Deuzé, J.L., Diner, D.J., Dubovik, O., Ducos, F., Emde, C., et al., 2010. The inter-comparison of major satellite aerosol retrieval algorithms using simulated intensity and polarization characteristics of reflected light. *Atmos. Meas. Tech.* 3 (4), 909–932. <https://doi.org/10.5194/amt-3-909-2010>.
- Kulmala, M., Suni, T., Lehtinen, K.E.J., Dal Maso, M., Boy, M., Reissell, A., et al., 2004. A new feedback mechanism linking forests, aerosols, and climate. *Atmos. Chem. Phys.* 4 (2), 557–562. <https://doi.org/10.5194/acp-4-557-2004>.
- Levelt, P.F., Hilsenrath, E., Leppelmeier, G.W., Oord, G.H.J., Bhartia, P.K., Tamminen, J., et al., 2006. Science objectives of the ozone monitoring instrument. *IEEE Trans. Geosci. Remote Sens.* 44 (5), 1199–1208. <https://doi.org/10.1109/TGRS.2006.872336>.
- Levy, R.C., Remer, L.A., Mattoo, S., Vermote, E.F., Kaufman, Y.J., 2007. Second-generation operational algorithm: retrieval of aerosol properties over land from inversion of moderate resolution imaging Spectroradiometer spectral reflectance. *J. Geophys. Res. Atmos.* 112 (D13) <https://doi.org/10.1029/2006JD007811>.
- Levy, R.C., Mattoo, S., Munchak, L.A., Remer, L.A., Sayer, A.M., Patadia, F., Hsu, N.C., 2013. The collection 6 MODIS aerosol products over land and ocean. *Atmos. Meas. Tech.* 6 (11), 2989–3034. <https://doi.org/10.5194/amt-6-2989-2013>.
- Levy, R.C., Munchak, L.A., Mattoo, S., Patadia, F., Remer, L.A., Holz, R.E., 2015. Towards a long-term global aerosol optical depth record: applying a consistent aerosol retrieval algorithm to MODIS and VIIRS-observed reflectance. *Atmos. Meas. Tech.* 8 (10), 4083–4110. <https://doi.org/10.5194/amt-8-4083-2015>.
- Li, X., Strahler, A.H., 1992. Geometric-optical bidirectional reflectance modeling of the discrete crown vegetation canopy: effect of crown shape and mutual shadowing. *IEEE Trans. Geosci. Remote Sens.* 30 (2), 276–292. <https://doi.org/10.1109/36.134078>.
- Li, Z., Zhao, X., Kahn, R., Mishchenko, M., Remer, L., Lee, K.-H., et al., 2009. Uncertainties in satellite remote sensing of aerosols and impact on monitoring its long-term trend: a review and perspective. *Ann. Geophys.* 27 (7), 2755–2770. <https://doi.org/10.5194/angeo-27-2755-2009>.
- Li, J., Kahn, R.A., Wei, J., Carlson, B.E., Laci, A.A., Li, Z., et al., 2020. Synergy of satellite- and ground-based aerosol optical depth measurements using an ensemble Kalman filter approach. *J. Geophys. Res. Atmos.* 125 (5) <https://doi.org/10.1029/2019JD031884>.
- Litvinov, P., Hasekamp, O., Cairns, B., 2011a. Models for surface reflection of radiance and polarized radiance: comparison with airborne multi-angle photopolarimetric measurements and implications for modeling top-of-atmosphere measurements. *Remote Sens. Environ.* 115 (2), 781–792. <https://doi.org/10.1016/j.rse.2010.11.005>.
- Litvinov, P., Hasekamp, O., Cairns, B., Mishchenko, M., 2011b. Semi-empirical BRDF and BPDF models applied to the problem of aerosol retrievals over land: Testing on airborne data and implications for modeling of top-of-atmosphere measurements. In: *Polarimetric Detection, Characterization and Remote Sensing*. Springer, Dordrecht, pp. 313–340. https://doi.org/10.1007/978-94-007-1636-0_13.
- Litvinov, P., Dubovik, O., Chen, C., Torres, B., Dubovik, I., Fuentes, D., Lopatin, A., Lapyonok, T., Herreras, M., Derimian, Y., Herrera, M., 2020. Combined retrieval from ground based and space-borne measurements: new possibilities for surface validation and beyond. In: *AGU Fall Meeting Abstracts*, vol. 2020 pp. A208-06.
- Litvinov, P., Chen, C., Matar, C., Bindreiter, L., et al., 2022. Synergetic retrieval from Ground-based and Satellites measurements: new possibilities for surface characterization and validation – Final Report (FR).
- Litvinov, P., Chen, C., Dubovik, O., Bindreiter, L., Matar, C., et al., 2024. Extended aerosol and surface characterization from SSP/TROPOMI with GRASP algorithm. Part I: Conditions, approaches, performance and new possibilities. *Remote Sens. Environ.* 114355 <https://doi.org/10.1016/j.rse.2024.114355>.
- Llewellyn-Jones, D., Edwards, M.C., Mutlow, C.T., Birks, A.R., Barton, I.J., Tait, H., 2001. AATSR: global-change and surface-temperature measurements from Envisat. *ESA Bull.* 105 (10–21), 25.
- Lopatin, A., Dubovik, O., Fuentes, D., Stenchikov, G., Lapyonok, T., Veselovskii, I., et al., 2021. Synergy processing of diverse ground-based remote sensing and in situ data using GRASP algorithm: applications to radiometer, lidar and radiosonde observations. *Atmos. Meas. Tech.* 14, 2575–2614. <https://doi.org/10.5194/amt-14-2575-2021>.
- Lyapustin, A., Wang, Y., Korkin, S., Huang, D., 2018. MODIS collection 6 MAIAC algorithm. *Atmos. Meas. Tech.* 11, 5741–5765. <https://doi.org/10.5194/amt-11-5741-2018>.
- Mahowald, N.M., Scanza, R., Brahney, J., Goodale, C.L., Hess, P.G., Moore, J.K., Neff, J., 2017. Aerosol deposition impacts on land and ocean carbon cycles. *Curr. Clim. Chang. Rep.* 3 (1), 16–31. <https://doi.org/10.1007/s40641-017-0056-z>.
- Monahan, E.C., O’Muircheartaigh, L., 1980. Optimal power-law description of oceanic whitecap coverage dependence on wind speed. *J. Phys. Oceanogr.* 10 (12), 2094–2099. [https://doi.org/10.1175/1520-0485\(1980\)010<2094:OPLDOO>2.0.CO;2](https://doi.org/10.1175/1520-0485(1980)010<2094:OPLDOO>2.0.CO;2).
- O’Neill, N.T., Eck, T.F., Smirnov, A., Holben, B.N., Thulasiraman, S., 2003. Spectral discrimination of coarse and fine mode optical depth. *J. Geophys. Res. D Atmos.* 108 (17) <https://doi.org/10.1029/2002jd002975>.
- Popp, T., de Leeuw, G., Bingen, C., Brühl, C., Capelle, V., Chedin, A., et al., 2016. Development, production and evaluation of aerosol climate data records from European satellite observations (Aerosol_cci). *Remote Sens.* 8 (5), 421. <https://doi.org/10.3390/rs8050421>.
- Pöschl, U., 2005. Atmospheric aerosols: composition, transformation, climate and health effects. *Angew. Chem. Int. Ed.* 44 (46), 7520–7540. <https://doi.org/10.1002/anie.200501122>.
- Rast, M., Bézy, J.L., Bruzzi, S., 1999. The ESA medium resolution imaging spectrometer MERIS a review of the instrument and its mission. *Int. J. Remote Sens.* 20 (9), 1681–1702. <https://doi.org/10.1080/014311699212416>.
- Remer, L.A., Kaufman, Y.J., Tanré, D., Mattoo, S., Chu, D.A., Martins, J., et al., 2005. The MODIS aerosol algorithm, products, and validation. *J. Atmos. Sci.* 62 (4), 947–973. <https://doi.org/10.1175/JAS3385.1>.
- Remer, Lorraine A., Levy, R.C., Mattoo, S., Tan, D., Gupta, P., Shi, Y., et al., 2020. The dark target algorithm for observing the global aerosol system: past, present, and future. *Remote Sens.* <https://doi.org/10.3390/rs12182900>.
- Ross, J., 1981. *The Radiation Regime and Architecture of Plant Stands. The Radiation Regime and Architecture of Plant Stands*. Dr W. Junk Publishers, The Hague, Netherlands.
- Salomonson, V., Barnes, W., Xiong, J., Kempfer, S., Masuoka, E., 2002. An overview of the earth observing system MODIS instrument and associated data systems performance. *Int. Geosci. Remote Sens. Sympos.* 2 (C), 1174–1176. <https://doi.org/10.1109/igars.2002.1025812>.
- Sayer, A.M., Munchak, L.A., Hsu, N.C., Levy, R.C., Bettenhausen, C., Jeong, M.-J., 2014. MODIS collection 6 aerosol products: comparison between Aqua’s e-deep blue, dark target, and “merged” data sets, and usage recommendations. *J. Geophys. Res. Atmos.* 119 (24), 13,965–13,989. <https://doi.org/10.1002/2014JD022453>.
- Sayer, A.M., Hsu, N.C., Bettenhausen, C., Jeong, M.-J., 2013. Validation and uncertainty estimates for MODIS Collection 6 “Deep Blue” aerosol data. *J. Geophys. Res. Atmos.* 118, 7864–7872. <https://doi.org/10.1002/jgrd.50600>.
- Sayer, A.M., Hsu, N.C., Lee, J., Bettenhausen, C., Kim, W., v., & Smirnov, A., 2018a. Satellite Ocean aerosol retrieval (SOAR) algorithm extension to S-NPP VIIRS as part of the “deep blue” aerosol project. *J. Geophys. Res. Atmos.* 123 (1), 380–400. <https://doi.org/10.1002/2017JD027412>.
- Sayer, A.M., Hsu, N.C., Lee, J., Kim, W., Dubovik, O., Dutcher, S.T., et al., 2018b. Validation of SOAR VIIRS over-water aerosol retrievals and context within the global satellite aerosol data record. *J. Geophys. Res. Atmos.* 123 (23) <https://doi.org/10.1029/2018JD029465>, 2018JD029465.
- Schaaf, C., Wang, Z., 2015a. MCD43C1 MODIS/Terra+Aqua BRDF/AlbedoModel Parameters Daily L3 Global 0.05Deg CMG V006 [Data set]. NASA EOSDIS Land Processes DAAC. Accessed 2020-09-14 from. <https://doi.org/10.5067/MODIS/MCD43C1.006>.
- Schaaf, C., Wang, Z., 2015b. MCD43C3 MODIS/Terra+Aqua BRDF/Albedo Albedo Daily L3 Global 0.05Deg CMG V006 [Data set]. NASA EOSDIS Land Processes DAAC. Accessed 2020-09-14 from. <https://doi.org/10.5067/MODIS/MCD43C3.006>.
- Schutgens, N., Sayer, A.M., Heckel, A., Hsu, C., Jethva, H., de Leeuw, G., et al., 2020. An AeroCom-AeroSat study: Intercomparison of satellite AOD datasets for aerosol model evaluation. *Atmos. Chem. Phys.* 20 (21), 12431–12457. <https://doi.org/10.5194/acp-20-12431-2020>.
- Schutgens, N., Dubovik, O., Hasekamp, O., Torres, O., Jethva, H., Leonard, P.J.T., 2021. AEROCOM and AEROSAT AOD and SSA study – Part 1 : Evaluation and intercomparison of satellite measurements. *Atmos. Chem. Phys.* 21 (9), 6895–6917. <https://doi.org/10.5194/acp-21-6895-2021>.
- Sinyuk, A., Holben, B.N., Eck, T.F., Giles, D.M., Slutsker, I., Korkin, S., et al., 2020. The AERONET version 3 aerosol retrieval algorithm, associated uncertainties and comparisons to version 2. *Atmos. Meas. Tech.* 13 (6), 3375–3411. <https://doi.org/10.5194/amt-13-3375-2020>.
- Smirnov, A., Holben, B.N., Eck, T.F., Dubovik, O., Slutsker, I., 2000. Cloud-screening and quality control algorithms for the AERONET database. *Remote Sens. Environ.* 73 (3), 337–349. [https://doi.org/10.1016/S0034-4257\(00\)00109-7](https://doi.org/10.1016/S0034-4257(00)00109-7).

- Sogacheva, L., Popp, T., Sayer, A.M., Dubovik, O., Garay, M.J., Heckel, A., et al., 2020. Merging regional and global aerosol optical depth records from major available satellite products. *Atmos. Chem. Phys.* 20 (4), 2031–2056. <https://doi.org/10.5194/acp-20-2031-2020>.
- Tanré, D., Kaufman, Y.J., Herman, M., Mattoo, S., 1997. Remote sensing of aerosol properties over oceans using the MODIS/EOS spectral radiances. *J. Geophys. Res. Atmos.* 102 (D14), 16971–16988. <https://doi.org/10.1029/96JD03437>.
- Tilstra, L.G., Tuinder, O.N.E., Wang, P., Stammes, P., 2017. Surface reflectivity climatologies from UV to NIR determined from Earth observations by GOME-2 and SCIAMACHY. *J. Geophys. Res.* 122 (7), 4084–4111. <https://doi.org/10.1002/2016JD025940>.
- Tilstra, Lieuwe G., Tuinder, O.N.E., Wang, P., Stammes, P., 2021. Directionally dependent Lambertian-equivalent reflectivity (DLER) of the Earth's surface measured by the GOME-2 satellite instruments. *Atmos. Meas. Tech.* 14 (6), 4219–4238. <https://doi.org/10.5194/amt-14-4219-2021>.
- Veefkind, J.P., Aben, I., McMullan, K., Förster, H., de Vries, J., Otter, G., et al., 2012. TROPOMI on the ESA Sentinel-5 precursor: A GMES mission for global observations of the atmospheric composition for climate, air quality and ozone layer applications. *Remote Sens. Environ.* 120 (2012), 70–83. <https://doi.org/10.1016/j.rse.2011.09.027>.
- Wielicki, B.A., Cess, R.D., King, M.D., Randall, D.A., Harrison, E.F., 1995. Mission to planet earth: role of clouds and radiation in climate. *Bull. Am. Meteorol. Soc.* 76 (11), 2125–2154. [https://doi.org/10.1175/1520-0477\(1995\)076<2125:mtpero>2.0.co;2](https://doi.org/10.1175/1520-0477(1995)076<2125:mtpero>2.0.co;2).